MAX-PLANCK-INSTITUT FÜR PLASMAPHYSIK

GARCHING BEI MÜNCHEN

Transport Code Predictions on the Performance of Lower Hybrid Heating in the ASDEX Tokamak

D. Eckhartt, A. McKenney

IPP 4/197
6/206

March 1981

Die nachstehende Arbeit wurde im Rahmen des Vertrages zwischen dem Max-Planck-Institut für Plasmaphysik und der Europäischen Atomgemeinschaft über die Zusammenarbeit auf dem Gebiete der Plasmaphysik durchgeführt.

TRANSPORT CODE PREDICTIONS ON THE PERFORMANCE OF LOWER HYBRID HEATING IN THE ASDEX TOKAMAK

D. Eckhartt and A. McKenney
Max-Planck-Institut fuer Plasmaphysik,
EURATOM-Association, D-8046 Garching

ABSTRACT

Lower Hybrid heating of an Ohmically heated plasma in the ASDEX tokamak is simulated by adding suitable power deposition terms to the 1-D BALDUR transport code. Ion heating by mode conversion and electron heating by Landau damping are considered as absorption mechanisms with the simplifying assumption that the spectral distribution of Lower Hybrid wave power remains unchanged on its passage through the plasma. Parameters of the wave heating scheme refer to the planned Lower Hybrid heating experiment in ASDEX.

1. Introduction

Plasma heating by absorption of microwave power will be investigated in the ASDEX tokamak with RF-powers of about 2 Megawatts at a frequency (1,3 GHz) in the lower hybrid (LH) range and heating times of 1..2 sec. In an ohmically heating "target" plasma, either preferential ion heating via mode conversion in a hydrogen plasma or preferential electron heating by Landau damping in a hydrogen-deuterium plasma is expected to occur at peak electron densities of $3....5 \times 10^{13} cm^{-3}$. This heating experiment is now under construction [1], and is planned to be operational by the end of 1982.

In order to assess the performance of these heating schemes in ASDEX, numerical calculations were made using the BALDUR 1-D tokamak transport code [2] with suitable terms added to describe, in a simplified manner, the deposition of microwave power into plasma ions and electrons. The immediate objective of these calculations was to obtain additional design criteria for the hardware of the heating experiment (that is, the microwave launching structure, or "grill").

It is obvious that the credibility of results from computer code predictions depends upon the following assumptions:

- that transport calculations, in general, are capable of describing the behaviour of magnetically confined toroidal plasmas in terms of heat and particle transport, impurity release, temperature and density profiles, etc.; this capability can be assessed, for example, by simulating the relatively simple Ohmic heating process and comparing the computations with the measured time and space evolutions of plasma parameters,
- that the various mechanisms of LH power absorption are correctly described by the existing theoretical approaches,
- that the concepts of wave launching and wave propagation through the plasma are valid and can be adequately modelled to enter the code computations.

These assumptions, together with other simplifications which are necessary to render the computational procedure tractable, imply a margin of incertainity in the results given in the following report. This proviso should be kept in mind when interpreting the results. They should rather be considered as a first step on the way towards refining the model calculations to such an extent, that the comparison between computational and experimental results could serve as a basis to get a more complete insight into the physics of wave launching, propagation, and absorption, as well as into possible modifications to the plasma transport resulting from wave-plasma interactions.

Similiar calculations were published recently [3,4], and fair agreement was claimed for electron heating in the former ATC-device [3].

In the following chapter, the physics of plasma heating by LH-waves is outlined. In Chapter 3 computer code calculations on Ohmic heating in the ASDEX tokamak are compared with experimental results. In Chapter 4 the modelling of LH wave power deposition will be described. This is followed by the results of computer predictions for preferential heating of ions and electrons, respectively.

2. Plasma Heating through Absorption of Lower Hybrid Waves

The heating of large tokamak plasmas up to reactor-grade conditions will be accomplished in several major steps:

- Ohmic heating will carry the plasma temperature to values somewhere below 1 keV.
- subsequent (or "additional") heating raises the temperature to values of about 10 keV where
- nuclear heating by charged fusion-reaction products takes over.

At the present time, work on heating is concentrated on bridging the gap between ~ 1 keV and ~10 keV without causing detrimental effects on plasma stability and cleanliness. Neutral beam heating has proved successful but will suffer from penetration problems with increasing plasma dimensions and plasma density. In addition, once ignition is reached, free-streaming of neutrons into the beam lines will seriously affect their maintainance. Plasma heating by radio-frequency electromagnetic fields with wave power deposition deep inside the plasma is another major candidate, but its viability at multi-mega-watt power levels has still to be demonstrated. Among the various possible RF heating schemes the lower hybrid range of frequencies has been found attractive as it offers a number of advantages from the engineering point of view:

- power sources are commercially available
- wave launching at the plasma edge does not require complicated antenna structures in the intererior of the vacuum vessel.

Lower hybrid heating has been extensively described in the literature [5,6]. It is characterised by the excitation and absorption of waves at a frequency ω which is related to the characteristic frequencies of a magnetically confined plasma ω_p (= plasma frequency) and ω_c (= cyclotron frequency) of the plasma particles (ions and electrons) in the following manner:

$$\omega_{ci} \ll \omega \approx \sqrt{\omega_{ci} \cdot \omega_{ce}} \ll \omega_{ce} \qquad (1)$$

and

$$\omega_{pi}\left(n_i(0)\right) \approx \omega \ll \omega_{pe}\left(n_e(0)\right) \qquad (2)$$

where n (o) denotes the peak particle density (at the plasma centre). Inspection of the dispersion relation which connects wave propagation (in

terms of frequency and wave numbers $k_{\parallel}$ and $k_{\perp}$ parallel and perpendicular to the magnetic confining field) and plasma properties, shows that, under these conditions, two modes of waves can propagate into the plasma (that is, in the direction of the density gradient and perpendicular to the magnetic confining field) when excited at the plasma edge. Of these, the slow mode is of more immediate interest for heating, since its perpendicular phase velocity inside the plasma can become small enough to allow efficient absorption by the ions; alternatively, efficient electron heating can be obtained by reducing the parallel phase velocity with an appropriate design of the antenna. At the low plasma densities near the plasma edge, this slow mode is so polarised as to have an electric field component $E_{\parallel}$ parallel to the static magnetic confining field. Thus, an antenna which is located at the plasma periphery and designed in such a way as to produce an $E_{\parallel}$ -field with parallel refractive index numbers $N_{\parallel} > 1$ ($N_{\parallel} = \frac{k_{\parallel} \cdot c}{\omega}$) can couple to this mode. When launched from such an antenna into a low density plasma ($n_e \leqslant 2{,}1 \times 10^{10} cm^{-3}$ for 1,3 GHz), the waves are at first evanescent until they reach regions of higher plasma density where they can freely propagate. This propagation occurs in geometrically well defined patterns ("resonance cones"): the direction of propagation, being nearly perpendicular to the static magnetic confining field at the plasma edge, it bent more and more in the direction of the magnetic field as the plasma density increases. When approaching the central parts of the plasma, the waves travel nearly parallel to the magnetic field lines, that is, tangential to the magnetic surfaces. On such a magnetic surface, plasma parameters such as density and temperature are almost constant (due to the free motion of plasma particles along the magnetic field lines). This change in the direction of wave propagation is related to a change in the magnitude of $k_{\perp}$, the wave number perpendicular to the magnetic confining field: when approaching the regions of higher density near the plasma centre, $k_{\perp}$ becomes larger and larger and, conversely, phase

velocity and wave-length perpendicular to the magnetic confining field get smaller and smaller.

When the perpendicular wave length is comparable to the ion gyro radius around the magnetic field lines, the wave propagation characteristics are strongly modified leading to mode conversion (or transformation) into a short wave-length ion wave. On the other hand, when $\frac{\omega}{k_\perp}$ becomes of the order of the thermal ion velocity, cyclotron resonance takes place, and by this mechanism wave power is converted into perpendicular ion energy. These two processes occur at about the same point.

Thus, the inward travelling LH-wave is absorbed near the location where this mode conversion takes place. This location, called the "linear turning point" (LTP), occurs at a value of the plasma electron density which is defined by the following implicit equation [7] for the plasma frequency ω_p of the different species in a multi-ion plasma [8]:

$$1 = \sum_j \frac{\omega_{pij}^2}{\omega^2} - \frac{\omega_{pe}^2}{\omega_{ce}^2} + N_{\parallel} \cdot \frac{v_{the}}{c} \left[6 \cdot \sum_j \frac{\omega_{pij}^2}{\omega_{pe}^2} \frac{\omega_{pe}^4}{\omega^4} \frac{v_{thij}^2}{v_{the}^2} + \frac{3}{2} \frac{\omega_{pe}^4}{\omega_{ce}^4} \right]^{1/2} \tag{4}$$

where j refers to the different ion species

and $v_{th} = \sqrt{\frac{2kT}{m}}$ denotes the thermal velocities of the various species.

For a single-ion plasma eq. (4) can be rewritten [9]:

$$\omega_{pi}^2 = \frac{\omega^2}{1 - \frac{\omega^2}{\omega_{ci} \cdot \omega_{ce}} + N_{\parallel} \cdot \frac{v_{the}}{c} \left[6 \frac{T_i}{T_e} + \frac{3}{2} \left(\frac{\omega^2}{\omega_{ci} \cdot \omega_{ce}} \right)^2 \right]^{1/2}} \tag{5}$$

which, in certain cases, can be simplified by dropping the second term ($\propto \frac{1}{B^4}$) in the square brackets to become only dependent on $N_{\parallel} T_i^{1/2}$ (and B). [10].

An equally powerful absorption mechanism is connected to the magnitude of the parallel phase velocity of the LH-waves: when $\frac{\omega}{k_{\parallel}}$ becomes of the order of the thermal electron velocity, Landau damping sets in and wave power is converted into kinetic energy of electrons moving along the magnetic lines of force at approximately the same speed as the parallel phase velocity of the LH wave. These "resonant" electrons exchange momentum with the wave, a process which leads to a flattening (or "plateau"-formation) in the distribution of parallel electron velocities and is counteracted by collisions tending to restore the equilibrium velocity distribution. It is this collisional transfer which determines the steady-state rate of wave power absorption by the electrons. This model has been worked out in a quasi-linear approach to yield a rate of power absorption per unit volume [11]:

$$P_{LD} = \alpha \cdot \frac{Z_i + 2}{2} \cdot \frac{\nu_0 \cdot n_e \cdot T_e}{(2\pi)^{1/2}} \cdot \ln\left[\frac{N_{\parallel 1}}{N_{\parallel 2}}\right] \cdot \exp\left[\frac{-c^2}{2 \cdot N_{\parallel 1}^2 \cdot v_{the}^2}\right] \qquad (6)$$

where $N_{\parallel 1}$ and $N_{\parallel 2}$ define the width of the LH-power spectrum, ν_0 is the collisional frequency, $v_{the}^2 = \frac{k \cdot T_e}{m_e}$.

α is a corrective factor obtained by numerically solving the two-dimensional Fokker-Planck equation [12,13]. Eq. (6) is valid provided that the parallel electric field strength of the wave exceeds a certain threshold value (such that in velocity space quasilinear diffusion due to the wave fields is larger than collisional diffusion), but this condition is readily satisfied in the present circumstances.

Other processes have been discussed as possible candidates for the absorption of LH wave power, but were not considered in the present report. Among those are stochastic heating of ions [14] to high energies followed by collisional

thermalisation - a mechanism which could explain the high energy tail in the ion velocity distribution often observed in experiments [15], as well as the excitation of parametric instabilities with subsequent absorption of the "daughter waves" for which experimental evidence was also found [16].

Inspecting eqs. (4) or (5) for mode conversion, and eq. (6) for Landau damping (in which the exponential is the dominating factor) shows the crucial role played by $N_{\parallel}$ (or $k_{\parallel}$), the wave index (or wave number, resp.) parallel to the magnetic field in those plasma regions where absorption takes place. Only in simple one-dimensional geometries (semi-infinite plane, or "slab", and shearless cylinder) is the value of $N_{\parallel}$ constant in space and equal to its value imposed by the launching structure at the plasma edge (the values of $N_{\perp}$ and $k_{\perp}$, resp., follow from the dispersion relation). In the complex geometry of a tokamak plasma, however, the values of $k_{\parallel}$ and $k_{\perp}$ vary for two reasons: the direction of the magnetic confining field vector changes due to variations of its poloidal and radial components (generated by plasma current and toroidal field ripple, resp.), secondly, the toroidal and poloidal wave numbers change with major and minor radius as a result of the "curved" geometry along these directions. The spatial variations of $k_{\parallel}$ and $k_{\perp}$ as the wave propagates from the launching structure towards the plasma interior can be calculated by "ray tracing" computations. They show an average decrease of the parallel wave numbers, which, in certain cases, becomes so large, that conversion to the "fast wave" with subsequent loss of wave power can occur [17].

In the simplified approach presented in the following report the spatial variations of $k_{\parallel}$ (and $N_{\parallel}$) have been neglected. For this case, the spectral distribution of LH-wave power in the plasma in $N_{\parallel}$ is determined solely by the properties of the antenna structure which is

situated at the plasma edge. This antenna consists of an array of identical rectangular and parallel wave guides with reduced heights --a so - called "grill". It emits a "bell-shaped" power spectrum (see Fig. 6) which is defined by

- the number of wave guides, h, of the grill
- the periodicity length, Δ, i.e., the spacing between the mid-planes of neighbouring wave-guides
- the phase-difference between waves in adjacent wave guides
- the power in each wave guide

For the case of equal powers but opposite phases in adjacent wave guides, the maximum power is emitted for the wave index number

$$\langle N_{\parallel} \rangle = \frac{1}{2} \cdot \frac{\lambda_0}{\Delta} \quad , \text{ where } \quad \lambda_0 = \frac{2\pi \cdot c_0}{\omega}$$

At both sides of this maximum the power drops to zero for parallel wave indices: $N_{\parallel} = \langle N_{\parallel} \rangle \pm \frac{1}{2} \Delta N_{\parallel}$, where $\Delta N_{\parallel}$ is given by

$$\Delta N_{\parallel} = \frac{4}{h} \langle N_{\parallel} \rangle = \frac{2}{h} \frac{\lambda_0}{\Delta}$$

3. The Ohmically Heated "Target Plasma" in the ASDEX Tokamak

3.1. Some Properties of the Transport Code

The particle and energy transport in the target plasma were computed using the one-dimensional transport code BALDUR [2]. A pure hydrogen plasma or a hydrogen/deuterium (50 / 50) plasma was assumed, except that a constant $\overline{Z_{eff}}$-value of 1,5 or 2,5 was used to compute the resistivity and the bremsstrahlung losses.

The particle transport consisted of:

- Alcator-scaling, i.e., a con tribution to the particle diffusion coefficient of $\frac{3 \cdot 10^{16}}{n_e(r)} \left[cm^{-1} sec^{-1}\right]$
- losses due to hydrogen recombination
- sources due to ionisation of neutral gas

The ion energy transport consisted of:

- neoclassical transport
- convection
- losses due to charge-exchange with neutral hydrogen
- electron-ion thermal equilibration
- lower-hybrid heating

The electron energy transport consisted of:

- neoclassical transport including Ware pinch
- Alcator scaling, i.e., a contribution to the conductivity of $\frac{2{,}5 \cdot 10^{17}}{n_e(r)} \left[cm^{-1} sec^{-1}\right]$
- essentially infinite electron thermal conductivity where $q(r) \lesssim 1$ *)
- convection
- losses due to ionisation, radiation, and bremsstrahlung
- electron-ion thermal equilibration
- ohmic heating
- lower hybrid heating

The numerical constants in the Alcator scaling contributions were calibrated by comparison with PULSATOR-results [18]. Ionisation and charge exchange were computed using a Monte-Carlo neutral gas model. The neutral influx was scaled so as to keep the total number of particles constant. T_i and T_e at the edge were held at 10 eV, the density at the edge at $3 \times 10^{12} cm^{-3}$ or 10 % of the initial central density, whichever was less. The plasma current was held constant.

---

*) q is the "safety factor"

3.2. Comparison Between Computations and Experimental Results for an Ohmically Heated ASDEX Plasma.

ASDEX is a large tokamak (major radius R_o = 165 cm, minor radius a = 40 cm) with a main magnetic field of up to 26 kGauss (on axis), which was brought into operation at the beginning of 1980 to study the control of impurities in tokamak discharges by means of a poloidal divertor [19]. For a number of discharges made in the "divertor mode" (reduced iron impurity content) with a plasma current of 242 kA and a main magnetic field of 22 kGauss (q(a)= 4.4), the measurements of density and temperatures were compared with computed data, taking the same values of plasma current and magnetic field as input to the code. Figs. 1 and 2 show measured values (scattered points) of peak electron and ion temperatures, as well as of the energy replacement time, [20], plotted vs. peak electron density in a hydrogen plasma together with computed values (connected by smooth curves). As the experimental values of $\overline{Z}_{eff}$ vary around an average of 2,39, the computer runs were made for $\overline{Z}_{eff}$-numbers of 1,5 and 2,5. In Figs. 3 to 5, normalised radial profiles of electron density and temperature [21] and of ion temperature [22] are given. Full curves indicate computed values. Experiments are shown by dashed curves (fit to the measured values [20]), and by the measured values themselves, both normalised to the fitted peak values (details are given in the legends to the figures). As seen from Figs. 1 and 2, the experimental energy replacement times and peak temperatures fall somewhat short of the computed values (perhaps indicating larger loss processes). There is good agreement for the relative profiles of electron density and temperature, whereas the measured ion temperature profile is somewhat broader than the computed one.

The general agreement, however, is considered good enough to use the transport code for the RF-heating calculations, in particular when considering the somewhat incomplete knowledge about the details of the absorption and power deposition mechanisms.

4. Modelling of LH-Wave Power Deposition

4.1. Ion Heating by Mode Conversion

As outlined in Para. 2, mode conversion occurs near the Linear-Turning-Point (LTP), which is located where the plasma density satisfies eq. (4). Rewriting this equation and solving for the electron density at the LTP in a plasma composed of protons and deuterons with the same ion temperature T_i, one obtains for a frequency of 1.3 GHz:

$$n_{e_{LTP}} = \frac{1}{0{,}259\left(\frac{\nu_H+1}{2}\right) - \frac{1{,}027}{B^2} + 0{,}0298 \cdot N_{\parallel} \cdot T_e^{1/2}\left[1{,}77\left(\frac{T_i}{T_e}\right)\frac{3\nu_H+1}{4} + \frac{6{,}96}{B^4}\right]^{1/2}} \quad (7)$$

where: n_e in units of $10^{13}\,cm^{-3}$

B in Tesla

T in keV

$$\nu_H = \frac{n_{H^+}}{n_e} \qquad \left(\text{and } \nu_D = \frac{n_{D^+}}{n_e} = 1 - \nu_H\right)$$

Setting $T_e = T_i$, eq. (7) can be displayed by a set of curves: $n_{e_{LTP}}$ vs. B, with $[N_{\parallel} \cdot T_e^{1/2}]$ as a parameter.

Let the target plasma be described by its distributions of density and temperatures along the minor radius r; $n_e(r)$, $T_e(r)$, $T_i(r)$, which are, in general, monotonically decreasing functions of r, as shown in the previous paragraph.

After setting $T_e(r)$ and $T_i(r)$ into eq. (7) and choosing a value of the parallel wave index $N_{\parallel}$, the locations of the turning points are determined by the identity:

$$n_e(r) \equiv n_{e_{LTP}}(r,\vartheta)\Big|_{N_{\parallel}} \quad (8)$$

where the (r,ϑ)-dependence of the right-hand side comes from the variation of the main magnetic field along the minor circumference (that is,

in ϑ-direction): $B = \frac{B_0 \cdot R_0}{R_0 + r \cdot \cos\vartheta}$ (B_0: field on axis)

(neglecting contributions from the poloidal magnetic field). Thus, eq. (8) describes the loci of the LTP`s as an egg-shaped curve (r,ϑ) in the minor cross-section, with maximum and minimum radial extensions in the equatorial plane at the inner (high field) side and the outer side, resp., of the torus. These two radii are taken to define a ring-shaped toroidal shell along the major circumference: we assume that that portion of wave power out of the LH-spectrum which is associated with the chosen value of $N_{\parallel}$, is uniformly distributed among the ions situated inside the volume of this toroidal annulus.

The assumption of uniform distribution of the absorbed wave power is justifiable on the following grounds:

i) it is known from ray tracing calculations that LH wave power launched from a point source at the plasma boundary propagates along helical trajectories which --when approaching regions of higher plasma density -- move very slowly in radial inward direction as compared to their spiralling motion along the major circumference. A toroidal surface (r= const) of constant density near the LTP-density is then completely encircled by ray trajectories with no preference to any point along either the major or minor circumferences: the LH power can be considered uniformly spread over this toroidal surface. Thus, the total wave power from the peripherical point source can be treated as being uniformly emitted by the inner vacuum vessel wall--the resulting wave power density being transported radially inwards;

ii) absorbed wave power will be converted into thermal energy of the ions*) which travel along the helical magnetic field lines on a magnetic

---

*) the wave power is deposited in the perpendicular motion but the code cannot distinguish between perpendicular and parallel temperatures

surface, r = const., this leads to the equipartition of absorbed power on such a surface and hence inside the volume of the toroidal shell.

The procedure of wave power deposition described above is applied to each value of $N_{\parallel}$ in the power spectrum of the LH-waves (or to a set of discrete values of $N_{\parallel}$ when approximating the smooth power spectrum by a histogram.) If $n_e(r)$ is too small to satisfy eq. (8), no power will be absorbed. In this manner the deposition profile of all the incoming LH-power is computed for the target plasma using the radial distributions of n_e, T_e and T_i. These distributions will change as a result of wave power absorption, hence the power deposition profiles have to be re- computed after each time step during the RF heating phase. Increasing temperatures lead to a decrease in $n_{e_{LTP}}$ (see eq.(7)), thus shifting the LTP`s and the power deposition regions towards the outer parts of the plasma column. This outward shift of the heating regions induces a steepening of the temperature gradients, thus increasing the heat loss fluxes. The resulting steady state power deposition profile is then determined by the final temperature distribution which itself is controlled by the balance between this power deposition and the increased heat losses.

At lower plasma densities "hollow" ion temperature profiles are generated by wave absorption in the outer plasma regions. Such profiles could give rise to microinstabilities leading to increased plasma and heat transports in these regions and a possible levelling out of the hollow profiles. No attempt has been made to include such effects.

4.2. Electron Heating by Landau Damping

According to the quasi-linear theory, the power density dissipated by LH waves in the spectral range $N_{\parallel 1} \ldots N_{\parallel 2}$ due to Landau damping of

electrons, is given by eq. (6), which can be re-written in practical units (for $Z_i = 1$) as follows [23]:

$$P_{LD}(r, N_{\parallel 1}, N_{\parallel 2}) = 0{,}467 \cdot 10^{-24} \cdot \frac{n_e^2}{\sqrt{T_e}} \cdot \ln\left[\frac{N_{\parallel 1}}{N_{\parallel 2}}\right] \cdot \exp\left[-\frac{255{,}9}{N_{\parallel 1}^2 \cdot T_e}\right] \quad (9)$$

with p_{LD} in $W \cdot cm^{-3}$

n_e in cm^{-3}

T_e in keV

where $n_e(r)$ and $T_e(r)$ are the radial profiles of electron density and temperature, resp., in the target plasma. As this rate of power dissipation is independent of the incident wave power (or RF field amplitude), and as the energy absorbed from the wave is thought to be instantaneously shared between all the electrons on a magnetic surface (that is inside a toroidal annulus r...r+dr), the absorption process can be treated as axisymmetric around the major and minor circumferences. Thus, the total power P dissipated in the spectral range $N_{\parallel 1}...N_{\parallel 2}$ by a wave on its way from the plasma edge (r=a) to a radial position r is given (in cylindrical approximation) by

$$P(r, N_{\parallel 1}, N_{\parallel 2}) = \int_r^a P_{LD}(r', N_{\parallel 1}, N_{\parallel 2}) \, 4\pi^2 R_0 \, r' \, dr' \quad (10)$$

At the radius of furthest wave penetration, $r=r_c$, the total dissipated power according to eq. (10) equals the incident power.

In order to compute the power deposition profile, p_{LD} and P are computed at each radius r for a small interval of the $N_\parallel$-spectrum. By comparing P (r) with the wave power launched at the plasma edge, r_c can be found. This procedure is carried out for the entire spectrum. Summing up p_{LD} determines the wave power density deposited at a location r in the electrons.

In the calculations presented in the following paragraph, mode conversion and electron Landan damping take place simultaneously. The relative share of absorbed power between the two mechanisms depends largely on the number value of $N_{\parallel}$. If mode conversion occurs at a radius larger than r_c, the remainder of the wave power is deposited into the ions by the procedure described in the preceding section.

5. Results of Computations on LH-Heating in ASDEX and Discussion

5.1. Choice of Parameters

The heating effect due to LH power absorption depends on a number of parameters describing the properties of the "target plasma" as well as those of the HF-system. In the list below, "standard" values (which correspond to the expected regime of nominal operation during the RF-heating experiment) for these parameters are given as well as a number of variations around these standard parameters. These variations are used to study the response of the heating scheme to small changes of these parameters.

For a given set of parameters, the heating effect, measured in terms of central temperature variation, increase in ß, etc., is studied as a function of the peak electron density (by varying the filling pressure) measured at the instant of time (0.4 sec) when the RF-power is switched on (the peak density decreases slightly during the RF-heating phase as a result, probably, of a change in transport properties).

Working gas: H_2, or a mixture of equal parts of H_2 and D_2. In such a mixture, mode conversion is expected at somewhat higher densities than in a pure hydrogen plasma (c.f. eq. (7) for $\gamma_H < 1$); thus, preferential electron heating by Landau Damping can be studied at reasonably high plasma densities.

Plasma current: 346 kA
Main magnetic field: 25 kGauss } q (a) = 3.5

(or 242 kA and 22 kGauss, q(a)= 4.4, which are nominal values for the present operation of ASDEX)

$\bar{Z}_{eff}$: 1.5 (or 2,5)

LH-Wave power: 1 MW (or 0.5 ... 2 MW) radiated into the plasma

Power spectrum: three different power spectra were used in the numerical calculations (see Fig. 6). They correspond to different types of launching structures (or grills) and are denoted by their minimum and maximum $N_{\parallel}$-numbers:

(1) $N_{\parallel}$ = 2.1 ... 3.9, with $\langle N_{\parallel} \rangle \approx 2.9$, generated by 8 waveguides

(2) $N_{\parallel}$ = 2.3 ... 4.5, with $\langle N_{\parallel} \rangle \approx 3.1$, generated by 6 waveguides

these two grills are intended for preferential ion heating.

(3) $N_{\parallel}$ = 3,75 ... 6,25 with $\langle N_{\parallel} \rangle \approx 5$, generated by 8 wave-guides, for preferential electron heating

(In Fig. 20 variants to this power spectrum were used, obtained by dividing the $N_{\parallel}$-numbers by a constant number, thus "squeezing" or "extending" the $N_{\parallel}$-axis but leaving the relative power spectrum unchanged).

5.2. Preferential Heating of Ions

5.2.1 Standard Parameters

In Fig. 7 are shown the increase of the central ion and electron temperatures in a H_2-plasma resulting from the absorption of 1 MW of RF-power by the ions via mode conversion, plotted as a function of central electron density, together with the peak temperatures of the ohmically heated target plasma at the time (0.4 sec) when the RF power is applied. The T(o) vs. n_e (o) dependence follows a typical pattern: a sudden increase occurs when the peak electron density of the target plasma reaches a value roughly equal to the turning point density (eq. (7)) for values $N_{\parallel} \cdot \sqrt{T_e}$ which correspond, respectively, to the peak electron temperature of the target plasma and to the maximum $N_{\parallel}$ in the power spectrum. With increasing peak electron densities, the central temperature increases get smaller and smaller, but in such a way that the increases in total plasma energy - as expressed by the ß-values - stay constant (see Fig. 8). A typical evolution of the power deposition profile is shown in Fig. 9: as the plasma is heated and the temperatures increase the linear turning point shifts towards the outer part of the plasma. As a result of this outward shift, the ion temperature develops a hollow profile (see Fig. 10). The electrons, on the other hand, retain their monotonically decreasing temperature profiles (see Fig. 11) by "filling in" the central hole in the temperature profile through their high thermal conductivity inside the $q \leq 1$-surface. These changes are accompanied by a small drop in the central electron density (the total number of electrons being kept constant by the code).

With increasing filling pressures (or central densities), the steady-state radial position of maximum power deposition moves outwards (that is, towards

larger values of r). Thus the density of deposited power is decreased and spread among more particles. In addition, the power losses tend to become larger when the ion temperature is raised at the plasma edge. Both effects lead to the gradual decrease of central temparatures at higher densities seen in Fig. 7.

5.2.2. Variation of RF Input Power

The Ohmic heating power required to maintain the target plasma for the conditions of Fig. 7 amounts to about 400 kW. It drops to 1/3 or 1/2 of this value (depending on density) when 1 MW of RF power is switched on - thus representing only 1/8 to 1/6 of the total power input to the plasma (the plasma current being kept constant by the code). The resulting modification in the overall power deposition results in a change in the global energy replacement times, these --in comparison with Ohmic heating alone-- becoming somewhat longer at low densities but shorter at high densities.

A similar behaviour is seen when, for a given target plasma, different RF powers are used (see Fig. 12). The relative contribution due to Ohmic heating power drops to 5 % at the highest RF power level. At the same time, the relative share of the various power loss processes changes: at the highest RF power most of the power is lost via charge exchange (in the outer plasma regions), in contrast to low RF power levels, where electron conduction is the dominant loss mechanism (as with Ohmic heating alone). This re-arrangement of power deposition and subsequent modification of the relative power loss contributions could explain why the quantities shown in Fig. 12 as a function of absorbed microwave power deviate from linearity and tend to level off at high RF-powers.

5.2.3. Variation of Plasma Current and MainMagnetic Field

When plasma current and main magnetic field are reduced (leaving all other parameters unchanged), the ion heating via mode conversion is affected as shown by Fig. 13. The reduced Ohmic heating due to the lower plasma current leads to a decrease in the peak temperatures attainable. Lower electron temperatures as well as lower magnetic fields shift the LTP-density towards higher values (viz. eq. (7)). The shift of the threshold density for the onset of ion heating as computed from eq. (7) is in good agreement with the observed one displayed in Fig. 13.

5.2.4. Variation of $\overline{Z_{eff}}$

Increasing the value of $\overline{Z_{eff}}$ from 1.5 to 2.5 produces somewhat higher peak tempratures in the Ohmic target plasma, as expected, but has no effect on the final central temperatures obtained by ion heating via mode conversion (see Fig. 14).

5.3. Preferential Heating of Electrons

5.3.1. Standard Parameter Regime

If the power spectrum is shifted towards higher $N_{\parallel}$-values the incoming LH wave power is absorbed by electron Landau damping at low plasma densities. This is shown in Fig. 15, where wave power with a spectrum centered around $\langle N_{\parallel} \rangle = 5$ is launched into a plasma composed of equal parts of hydrogen and deuterium ions. The plasma response is different from mode conversion heating, since the absorbed power density depends in a more complicated way on the target plasma parameters (quadratic in density, exponential in temperature). Only a small fraction (increasing with density, up to 14 %) of the incoming power is absorbed below $n(o) \approx 2 \times 10^{13} cm^{-3}$, whereas above this "threshold" all RF power is absorbed.

At higher densities the conditions for mode conversion are satisfied again and ion heating becomes the dominant absorption mechanism, i.e. that fraction of the incoming wave power which (on its radial inward propagation towards the mode conversion layer) is not absorbed by electron Landau damping will be dumped into the ions inside the mode conversion region.

5.3.2. Variation of RF Input Power

Varying the RF power into a target plasma whose conditions are close to the maximum electron heating of Fig. 15 (i.e. for a central electron density of 2,87 x $10^{13}cm^{-3}$) gives the results shown in Fig. 16. As the RF-power is increased, the absorption zone is more and more shifted towards the plasma periphery, thus increasing the outward losses by electron heat conduction. This is reflected by the rapid decrease of the energy replacement times and could explain the relatively early levelling-off of the central ion temperature with increasing power: most of the power absorbed by the electrons is lost directly, since the density is too low for a good coupling between electrons and ions. By comparing these results with analogous results for mode conversion heating (see Fig. 12) it may be seen that (for the particular densities chosen) electron heating by Landau damping is less than half as efficient an absorption mechanism as measured by the increases in global thermal energy of the plasma (i.e., by the ß-values).

5.3.3. Variation of Plasma Current

By varying the plasma current, the electron temperature of the target plasma can be changed to a certain extent (other things such as plasma transport and extension of the $q \leq 1$-zone will change as well). An example of a change in plasma current and its effects on electron Landau damping is shown in Fig. 17. For the lower value of the plasma current, only a small fraction ($\lesssim 1$ %) of the incoming LH power is absorbed by electron

Landau damping. The results obtained for the higher plasma current resemble those of Fig. 15 except for the behaviour at densities below the onset of full Landau absorption: here a somewhat larger fraction of the incoming wave power is absorbed, thus making the transition to full power absorption somewhat smoother.

5.3.4. Variation of the Input Spectrum

The power spectrum of the incomping waves plays a decisive role due to the exponential dependence of the absorbed power density on $N_{\parallel}$ (cf. eq. 9). For the results shown in Fig. 18, the spectrum was chosen to range from $N_{\parallel} = 4.5 \ldots 7.5$ with a maximum at $\langle N_{\parallel} \rangle = 6$. Thus, electron heating sets in at relativley low densities, where electron-ion coupling is rather weak (which is apparent already in the Ohmically heated target plasma). In addition, the central density drops when LH power is absorbed by the electrons and their temperature rises (as usually observed). This could explain, why the central temperature is depressed even as compared with Ohmic heating alone. This "worsening" effect is overcome at central densities around $1{,}6 \times 10^{13} cm^{-3}$. At the high density end, mode conversion starts and leads to another increase in both ion and electron temperature at the centre.

By using a narrower $N_{\parallel}$-spectrum around the same $\langle N_{\parallel} \rangle$-value as that of Fig. 15, (doubling the number of grill wave guides) slightly better results are obtained, as seen from Fig. 19: maximum power transfer occurs at higher electron densities thus improving the coupling to the ions.

As mentioned before, the onset of full power absorption via Landau damping (at the density "treshold" of Fig. 15) is thought to be controlled by several counteracting mechanisms, affecting the electron temperature and density in the central region: electron heating by Landau damping ($\alpha\ n_e^2(o)$), radial expansion of the $q \lesssim 1$-zone with its subsequent temperature equali-

zation, density decrease as a result, probably, of a modification of Ware-pinch compression following the changes in temperature distribution. These effects can be accounted for by making a suitable choice of the power spectrum, whose $N_{\parallel}$-numbers enter exponentially into the absorbed power density (cf. eq. 9): the more the spectrum is shifted towards higher $N_{\parallel}$-numbers, the larger is the fraction of incoming LH-power absorbed. This is illustrated by Fig. 20, where the temperature increase in a fixed target plasma is plotted for different power spectra (indicated schematically at the bottom part of the figure) with constant total input power.

6. Summary of Conclusions

Transport calculations show that -- whith a suitable choice of the $N_{\parallel}$-spectra -- LH wave power will be deposited so as to heat either electrons or ions within the operating regime of an Ohmically heated target plasma in the ASDEX tokamak, that is, for central electron densities in the range 3 ... 6 x $10^{13}cm^{-3}$.Electron heating by Landau damping is found to be less efficient than preferential ion heating by mode conversion, as measured by the increases in total thermal energy (i.e. the β-values). Moreover, the observed temperature increases (up to 7 keV in T_i) do not grow linearly with absorbed wave power (up to 2 MW). Both effects can probably be explained by the peculiarities of LH wave power absorption together with the heat loss mechanisms in a tokamak plasma: LH wave power absorption can only occur within certain ranges of electron and ion temperatures whose locations, as a result of the rf-heating, are shifted towards the plasma periphery. Here, increased power losses by charge exchange (for the ions) and by steepened temperature gradients (for the electrons) carry the heat away before it is transferred to the central

plasma regions. There seems to be some room for optimisation (in particular for the regime of preferential electron heating) but this possibility has not been fully explored, since the modification of the LH power spectrum on its passage through the plasma was neglected in the present simplified approach.

7. Acknowledgements

We wish to thank the members of the RF-Heating Project and of the ASDEX Team for many useful discussions.

References

[1] H. Brinkschulte et al: "The Lower Hybrid Heating Programme for ASDEX", 2nd Joint Grenoble-Varenna Internat. Symposium on Heating in Toroidal Plasmas, Como, 3-12 September 1980

[2] D.E. Post, C.E. Singer, A.M. McKenney and the PPPL Transport Group: "Working Draft of the BALDUR Documentation", TFTR Physics Group Report Nr. 33 (January 1981), Princeton Plasma Physics Laboratory

[3] J. Ogden, S. Barnabei: "Transport Code Simulations of Lower Hybrid Heating in Tokamaks", Nuclear Fusion 20 (1980), p. 906

[4] E. Barbato, F. Santini,A. Taroni: "Simulation of Lower Hybrid Wave Propagation and Heating in Tokamak Discharges", 2nd Joint Grenoble-Varenna International Symposium on Heating in Toroidal Plasmas, Como,3 - 12 September 1980

[5] Project Staff - GAC-ANL: TNS Scoping Studies, Volume III, Reactor Physics: "Use of Lower Hybrid Heating to Reach Ignition", Report GA-A 14614, Vol. III, UC-20 d (January 1978)

[6] M. Brambilla: "The Feasibility of Igniting a Thermonuclear Plasma with Lower Hybrid Heating", Invited Paper, 2nd Joint Grenoble-Varenna Internat. Symposium on Heating in Toroidal Plasmas, Como, 3 - 12 September 1980

[7] P. Lallia: "Location of the Lower Hybrid Absorption Zone in Toroidal Devices", Report EUR-CEA-FC-774 (June 1975)

[8] Dr. F. Leuterer: Private Communication

[9] Reference [3], eq. (3)

[10] Reference [7], eq. (8)

[11] Ch. F.F. Karney, N.J. Fisch: "Numerical Studies of Current Generation by Radio Frequency Travelling Waves", Phys. Fluids 22 (1979) p. 1817., eq. (19)

[12] D.A. Ehst: "Design Constraints for Steady State Tokamak Reactors Driven by Lower Hybrid Waves", Nucl. Fusion 19 (1979) page 1369, see text after eq. (5)

[13] S.Y. Yuen, D. Kaplan, D.R. Cohn: "Characteristics of Lower-Hybrid-Wave-Driven Steady-State Tokamak Power Reactors", Nuclear Fusion 20 (1980), p. 159., see text after eq. (9)

[14] Ch. F.F. Karney: "Stochastic Ion Heating by a Lower Hybrid Wave", Phys. Fluids 21 (1978) p. 1584, and 22 (1979) p. 2188.

[15] C. Gormezano et al: "Lower Hybrid Heating Data on the WEGA-Experiment Revisited Using Ion Stochastic Heating and Landau Damping Theories", Report EUR-CEA-FC-1045 (1980)

[16] N. Suzuki et al: "Recent Results on the Modified JFT-2 Tokamak", 8th Intern. Conf. on Plasma Physics and Controlled Nuclear Fusion Research, Brussels, 1 - 10 July 1980, Paper IAEA-CN-38/T-2-3

[17] A. Cardinali, M. Brambilla: "Numerical Solution of the Ray Equations for Lower Hybrid Heating in a Tokamak", 2nd Joint Grenoble-Varenna, Internat. Sympos. on Heating in Toroidal Plasmas, Como, 3-12 Sept.1980

[18] Dr. D. Düchs: Private Communication

[19] M. Keilhacker et al: "Impurity Control Experiments in the ASDEX-Divertor Tokamak", 8th International Conference on Plasma Physics and Controlled Nuclear Fusion Research, Brussels, 1 - 10 July 1980, Paper IAEA-CN-38-O-1

[20] Courtesy Dr. H.-D. Murmann, ASDEX-Team, shots nr. 1604-07, 1617, 1619, 1620, 1612-14, 1621-29, 1601-03, 1609-11, 1594, 1596, 1598-99

[21] Shots nr. 1594, 1596, 1598, 1599

[22] Courtesy Dr. F. Wagner, ASDEX-Team: shots nr. 1605 - 1615

[23] Ref. [12], eq. (5), here the power density is given in watts per m^3,

Figure Captions

Fig. 1 Comparison between measured and computed peak temperatures in an Ohmically heated target plasma, plotted as a function of peak electron density. Peak electron and ion temperatures are shown by dots and crosses, respectively. Computed values are connected by fully drawn lines ($\overline{Z}_{eff}$ = 1.5) and dashed lines ($\overline{Z}_{eff}$ = 2.5) I_p = 242 kA, B_o = 22 kGauss

Fig. 2 Experimental and computed values of the energy replacement time, plotted as a function of peak electron density. Computations are shown by full curves, measurements by fuli dots.

Fig. 3 Comparison between computed and measured normalised radial profiles of the electron density. Computes values are shown by full curve with peak value $n_e(0) = 4.25 \times 10^{13} cm^{-3}$. Measurements are shown by open circles normalised to a central value of $4.16 \times 10^{13} cm^{-3}$ which is obtained by fitting the measurements to a smooth curve (dashed line connecting crosses)

Fig. 4 Comparison between computed and measured normalised radial profiles of the electron temperature measured at the same peak densities as in Fig. 3. Computed values are shown by the full curve (with a peak value of $T_e(0)$ = 0,76 keV). Measurements are shown by open circles normalised to a central value of 0,67 keV which is obtained by fitting the experimental values to a smooth curve (dashed curve connecting the crosses).

Fig. 5 Comparison between computed and measured normalised radial profiles of ion temperature. Computations refer to a peak electron density of 3,64 x $10^{13}cm^{-3}$, measurements are made at peak electron densities of 2.97 ... 3,75 x $10^{13}cm^{-3}$. Computed values are shown by full curve normalised to $T_i(o)$=0,69 keV. Measurements are shown by open circles at t = 0.55 sec., normalised to a peak value of 0.51 keV, and by open quadrangles at t = 1.0sec., normalised to a peak value of 0.59 keV.

Fig. 6 Normalised power spectra of the grill structures used in the numerical calculations. In the following text these spectra are referred to by their maximum and minimum $N_{\parallel}$-values

① : $N_{\parallel}$ = 2.1 ... 3.9

② : $N_{\parallel}$ = 2.3 ... 4.5

③ : $N_{\parallel}$ = 3.75 .... 6.25

Fig. 7 Computed central temperatures with and without LH heating of the ions via mode conversion. Central temperatures at the beginning (due to Ohmic heating) and at the end of the LH pulse (0.6 sec. duration) are plotted versus central density prior to the application of rf-power
H_2-plasma, I_{pl} = 346 kA, B_o = 25 kGauss,
$\overline{Z}_{eff}$ = 1.5, LH power: 1 MW, $N_{\parallel}$ = 2.1 .... 3.9.

Fig. 8 Volume averaged values of β_{pol} and β_{tor} as a function of peak electron density of the target plasma. Same parameters as for Fig. 7.

Fig. 9 Power deposition profiles (in watts per cm^3) for preferential ion heating via mode conversion. H_2-plasma, I_{pl} = 346 kA, B_o = 25 kGauss, $n_e(o)$ = 4.47 x $10^{13}cm^{-3}$, $\overline{Z}_{eff}$ = 1.5, LH power 1 MW, $N_{\parallel}$ = 2.1 ... 3.9.

Fig. 10 Ion temperature profiles, same conditions as for Fig. 9.

Fig. 11 Electron temperature profiles, same conditions as for Fig. 9.

Fig. 12 Plotted as a function of microwave power absorbed in a given target plasma are maximum ion temperatures $T_{i/max}$ (at the crest of the hollow radial profile), central temperature increases for ions ($\Delta T_i(o)$) and electrons($\Delta T_e(o)$), global energy replacement times τ_E, as well as increases in the volume averages of β_{pol} and β_{tor}. Peak electron density is $4.5 \times 10^{13} cm^{-3}$. Other conditions as in Fig. 7.

Fig. 13 Effect of changes in plasma current and main magnetic field on LH-heating with preferential ion heating via mode conversion. H_2-plasma, I_{pl} = 346 kA, B_o = 25 kGauss (full curves), I_{pl} = 242 kA, B_o = 22 kGauss (dotted curves), $\overline{Z}_{eff}$ = 1.5, LH power : 1 MW, $N_{\parallel}$ = 2,3 ... 4,5.

Fig. 14 Effect of $\overline{Z}_{eff}$ on LH-heating with preferential ion heating via mode conversion, H_2-plasma, I_{pl} = 242 kA, B_o = 22 kGauss, $\overline{Z}_{eff}$ = 1.5 (full curves), and $\overline{Z}_{eff}$ = 2.5 (dotted curves), LH-power : 1 MW, $N_{\parallel}$ = 2.3 ... 4.5.

Fig. 15 Preferential electron heating via Landau damping in a H_2 - D_2 plasma (50%-50%), I_{pl} = 346 kA, B_o = 25 kG, $\overline{Z}_{eff}$ = 1.5, LH power : 1 MW, $N_{\parallel}$ = 3.75 ... 6.25 upper curves refer to RF-heating, lower curves to Ohmic heating alone.

Fig. 16 Plotted as a function of microwave power absorbed by electron Landau damping in a given target plasma are: central temperature increases for electrons ($\Delta T_e(o)$) and ions ($\Delta T_i(o)$), global energy replacement times τ_E, as well as the increases in the volume averages of β_{pol} and β_{tor}. Peak electron density at the onset of the RF-heating pulse is $3.5 \cdot 10^{13} cm^{-3}$. Other conditions as in Fig. 15.

Fig. 17 Effect of changes in plasma current on LH-heating with preferential electron heating by Landau damping in a H_2-D_2 plasma (50%-50%). Upper set of curves: I_{pl} = 242 kA, B_o = 25 kGauss. Lower set of curves: I_{pl} = 403 kA, B_o = 25 kGauss, $\overline{Z}_{eff}$ = 1.5, LH power:1MW, $N_{\parallel}$ = 4.38 ... 5.63.

Fig. 18 Change of power spectrum and its effect on preferential electron heating by Landau damping in a H_2-D_2-plasma (50%-50%). I_{pl} = 242 kA, B_o = 22 kGauss, $\overline{Z}_{eff}$ = 1.5, LH power : 1 MW, $N_{\parallel}$ = 4.5 ... 7.5.

Fig. 19 Change of power spectrum (reducing its width) and its effect on preferential electron heating by Landau damping in a H_2-D_2-plasma (50 % - 50 %), I_{pl} = 34_6 kA, B_o = 25 kG, Z_{eff} = 1,5, LH-power: 1 MW, $N_{\parallel}$ = 4,35 .... 5,63.

Fig. 20 Variation of LH wave power spectrum near the onset of full power absorption by electron Landau damping in a given target plasma (H_2). Peak electron density at the onset of the RF-heating pulse is 2.23 x 10^{13} cm^{-3}, peak electron temperature is $T_e(o)$ = 1.05 keV. I_{pl} = 346 kA, B_o = 25 kGauss. Plotted are temperature increases *vs* $\langle N_{//} \rangle$, the $N_{//}$-number with maximum power density. Cross-hatched areas indicate extensions of the power spectra along the $N_{//}$-axis. LH power : 1 MW in all cases.

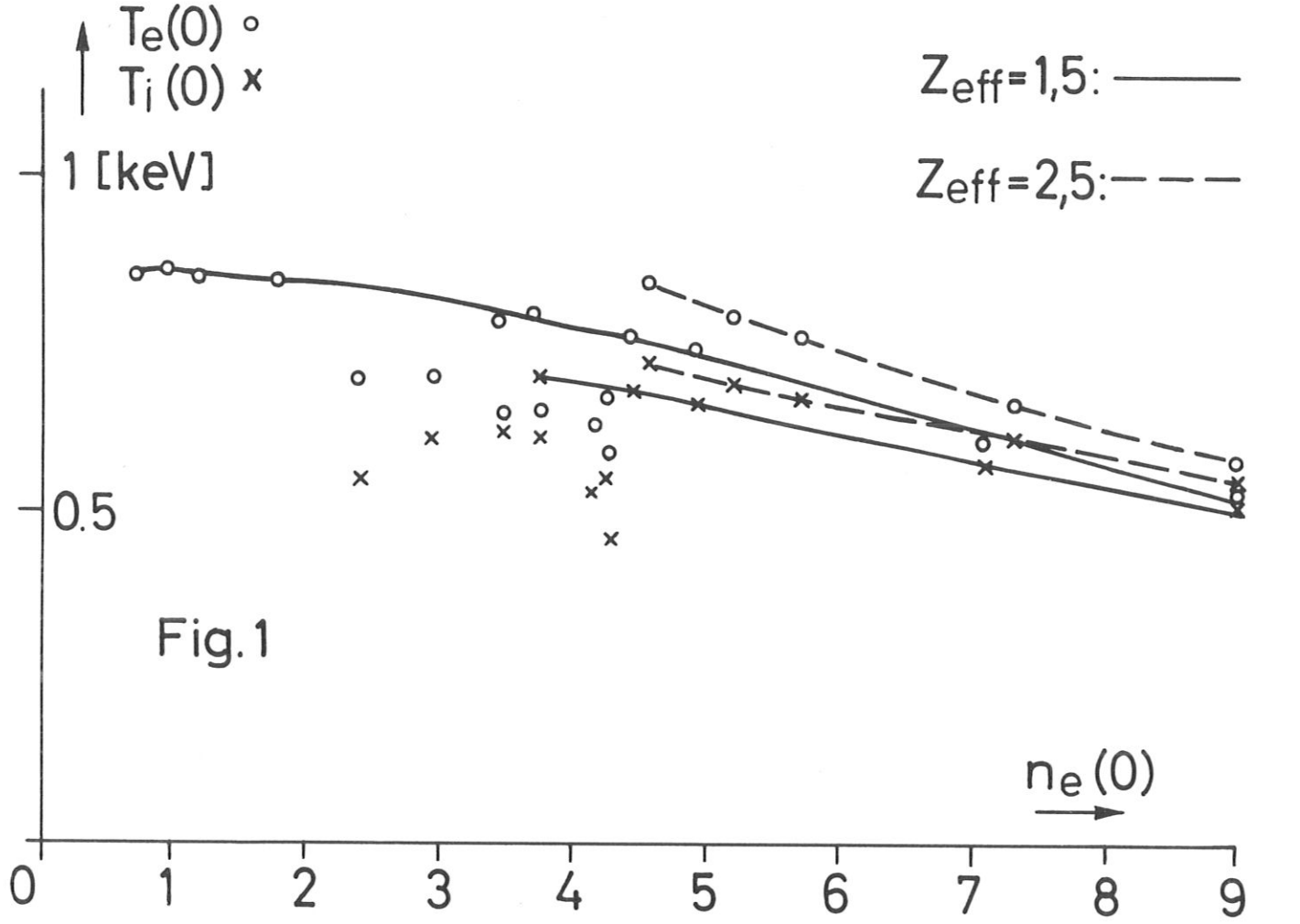
Te(0) °
Ti (0) x
Zeff=1,5: ——
Zeff=2,5:– – –
1 [keV]
0.5
ne (0)
0 1 2 3 4 5 6 7 8 9
x 10^13 [cm^-3]

Fig. 1

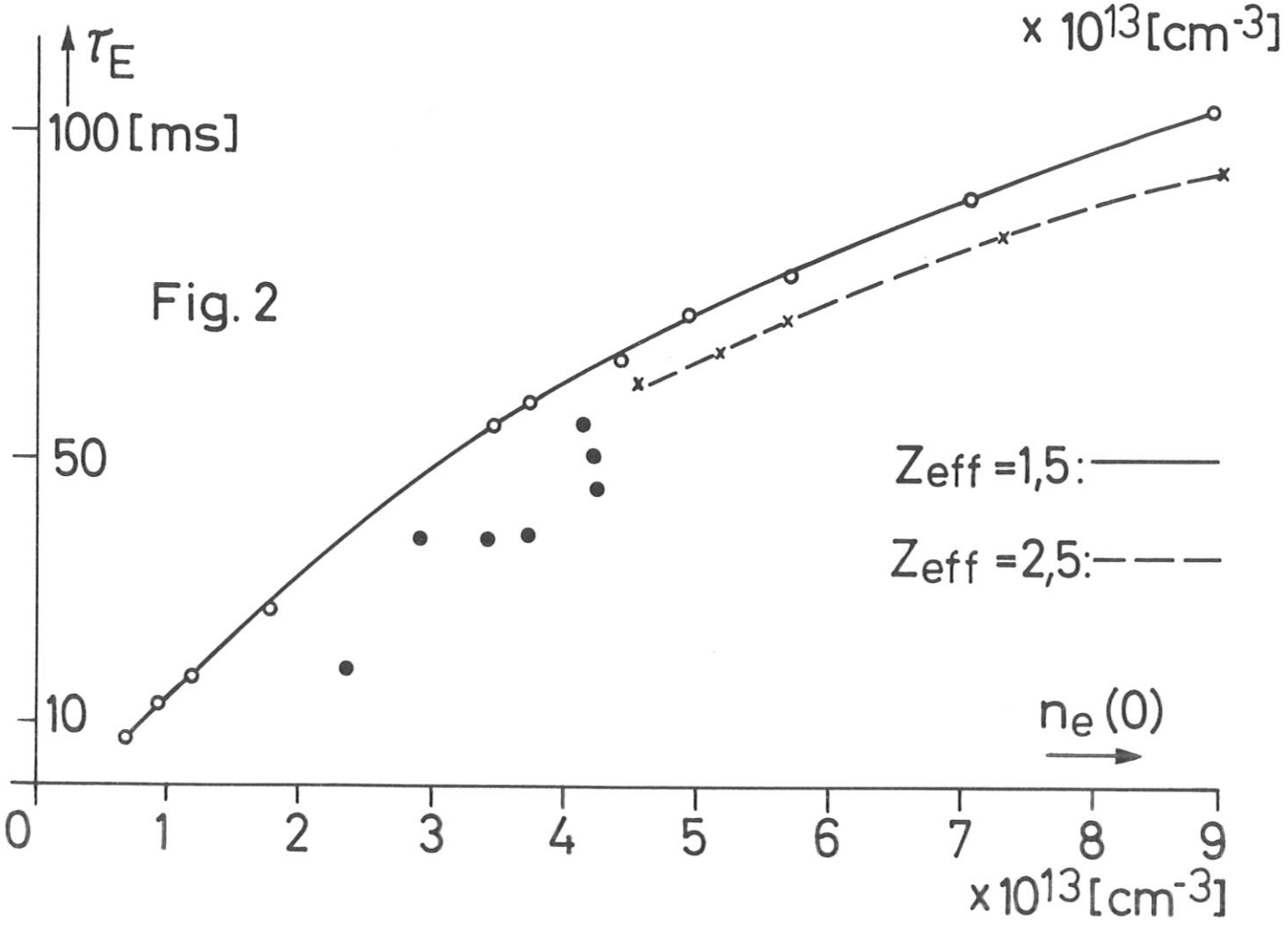
τE
100 [ms]
50
10
Zeff =1,5: ——
Zeff =2,5:– – –
ne (0)
0 1 2 3 4 5 6 7 8 9
x 10^13 [cm^-3]

Fig. 2

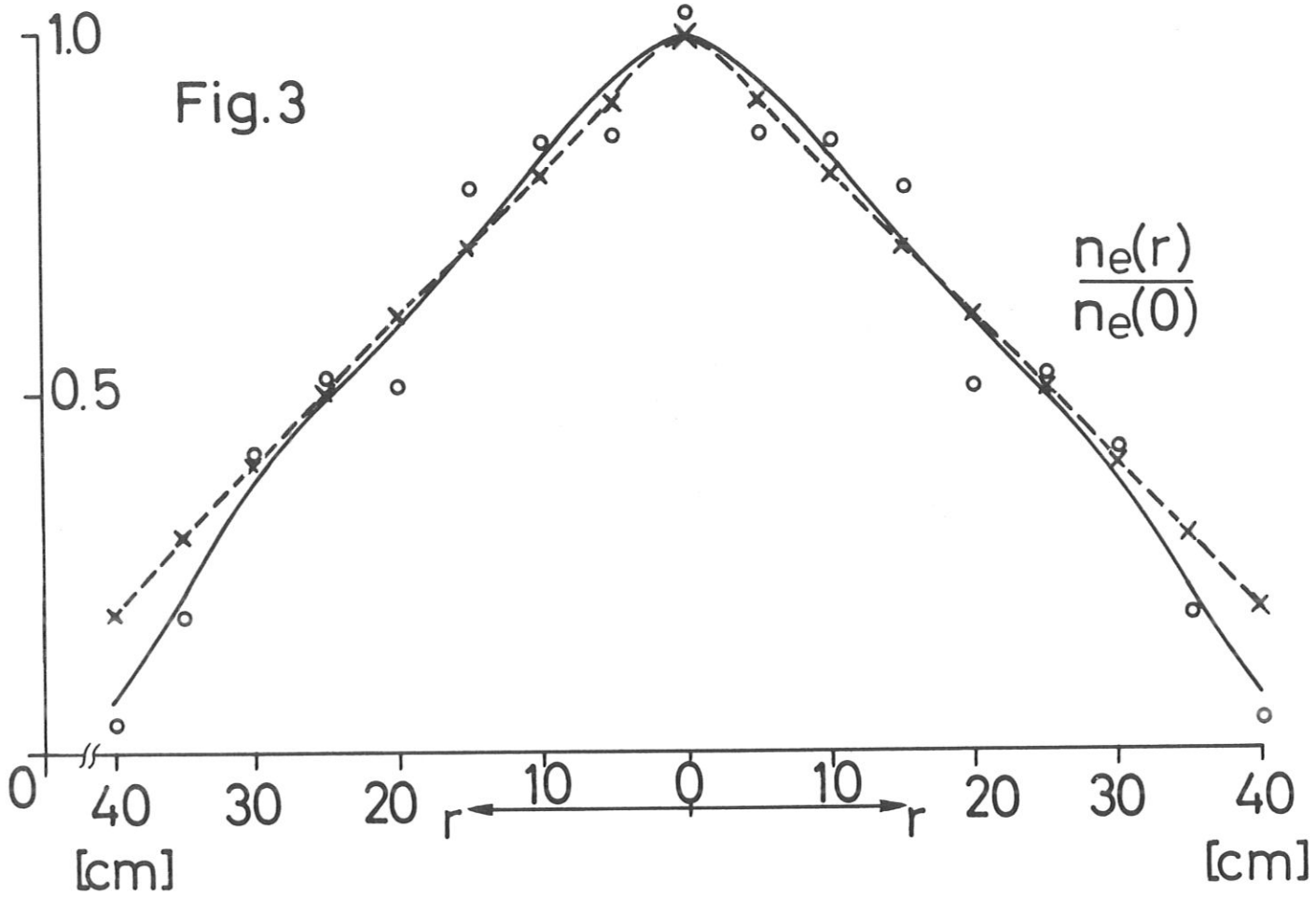
1.0
0.5
0
40
30
20
10
0
10
20
30
40
r
r
[cm]
[cm]
ne(r)
ne(0)

Fig.3

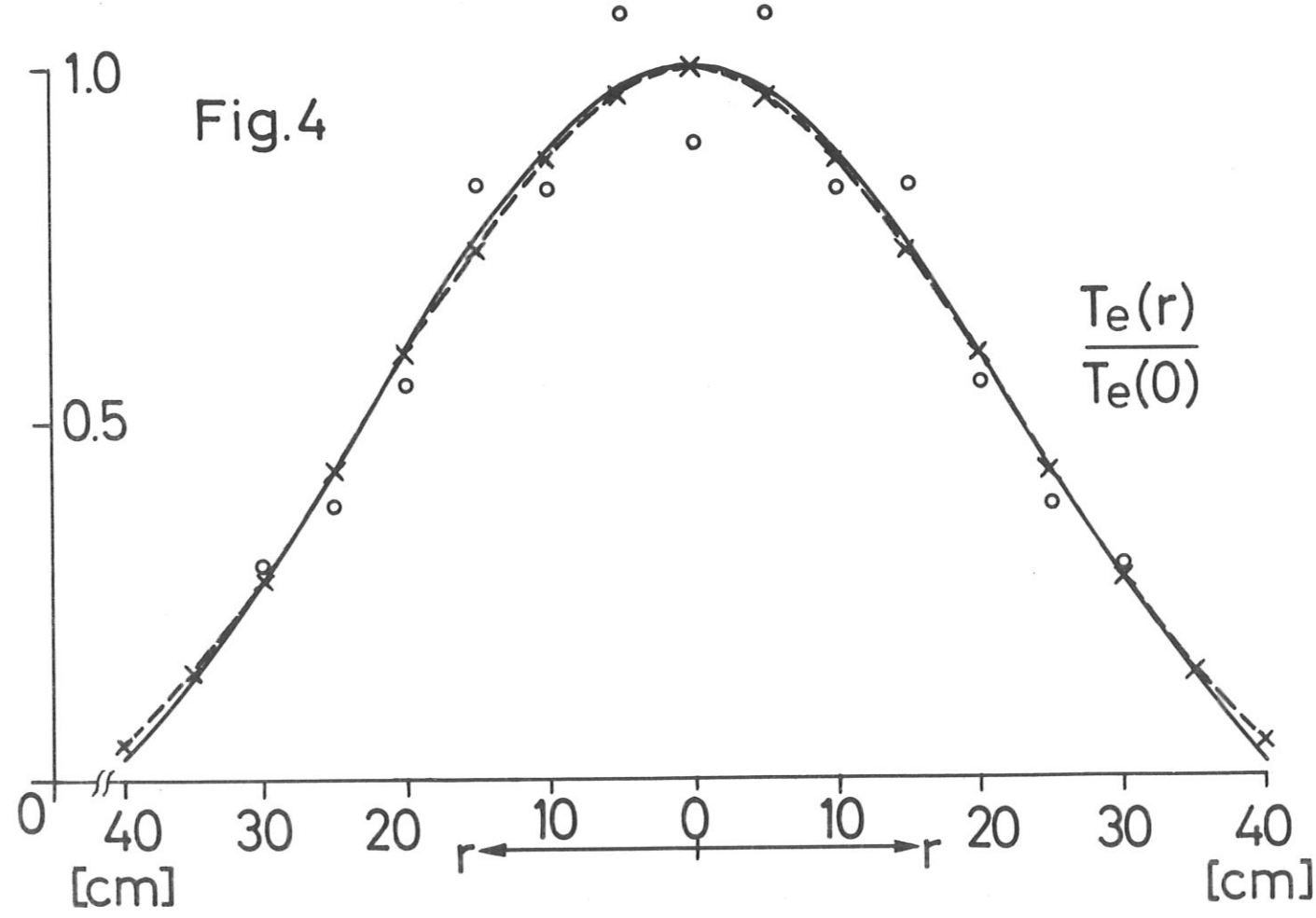
1.0
0.5
0
40
30
20
10
0
10
20
30
40
r
r
[cm]
[cm]
Te(r)
Te(0)

Fig.4

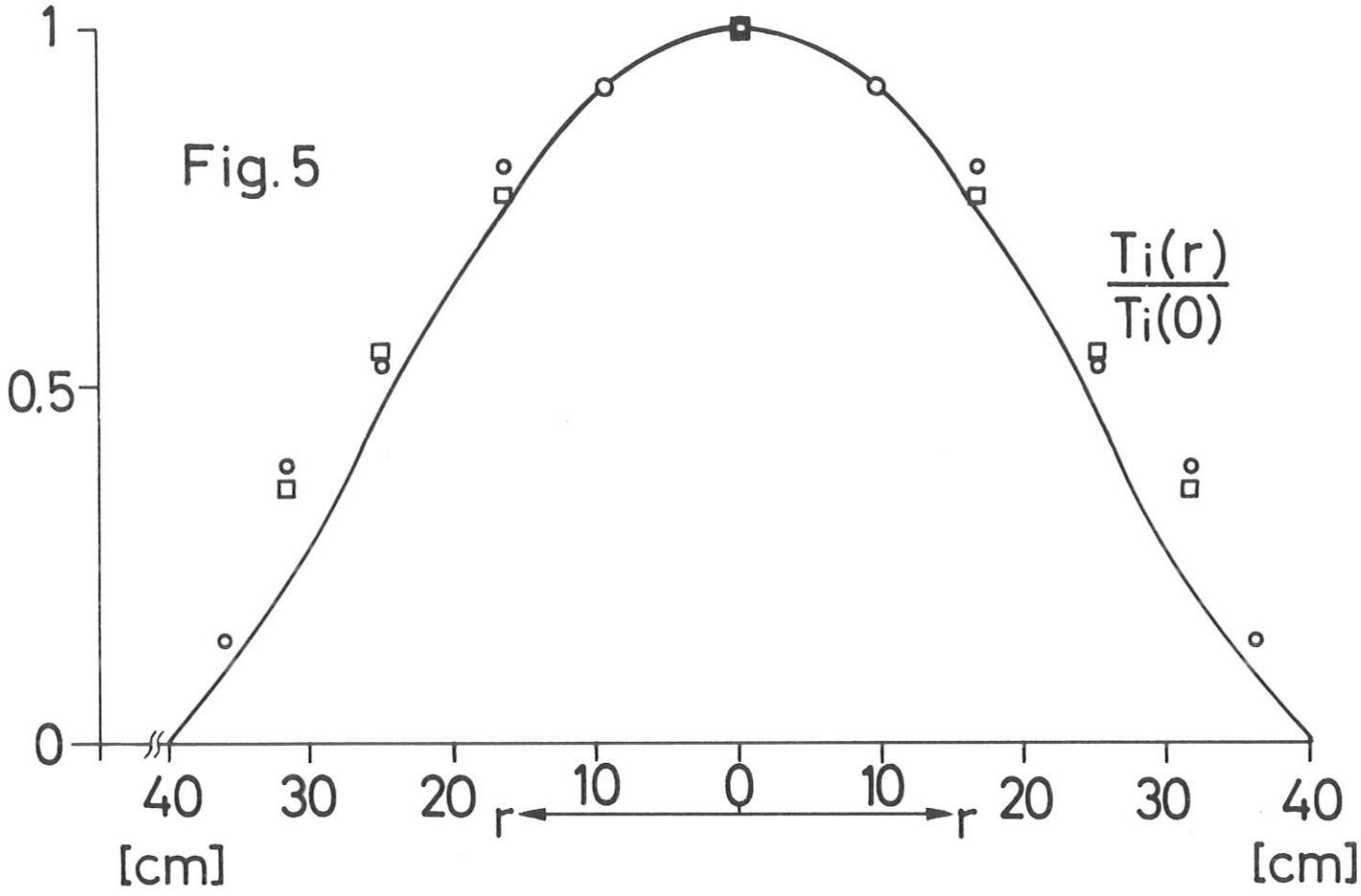
1
0.5
0
Ti(r)
Ti(0)
40
30
20
10
0
10
20
30
40
r
r
[cm]
[cm]

Fig. 5

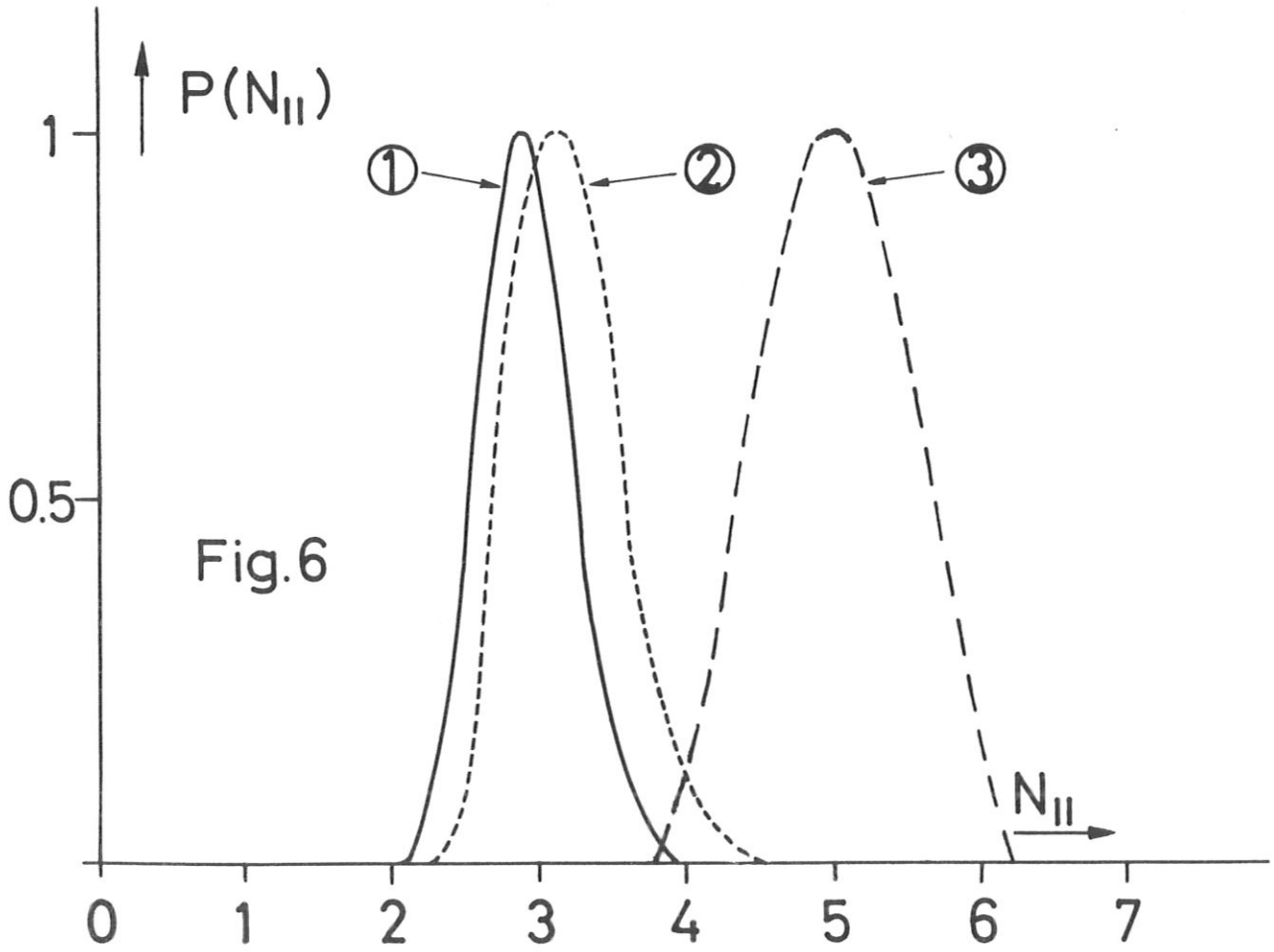
P(N∥)
1
0.5
①
②
③
N∥
0
1
2
3
4
5
6
7

Fig. 6

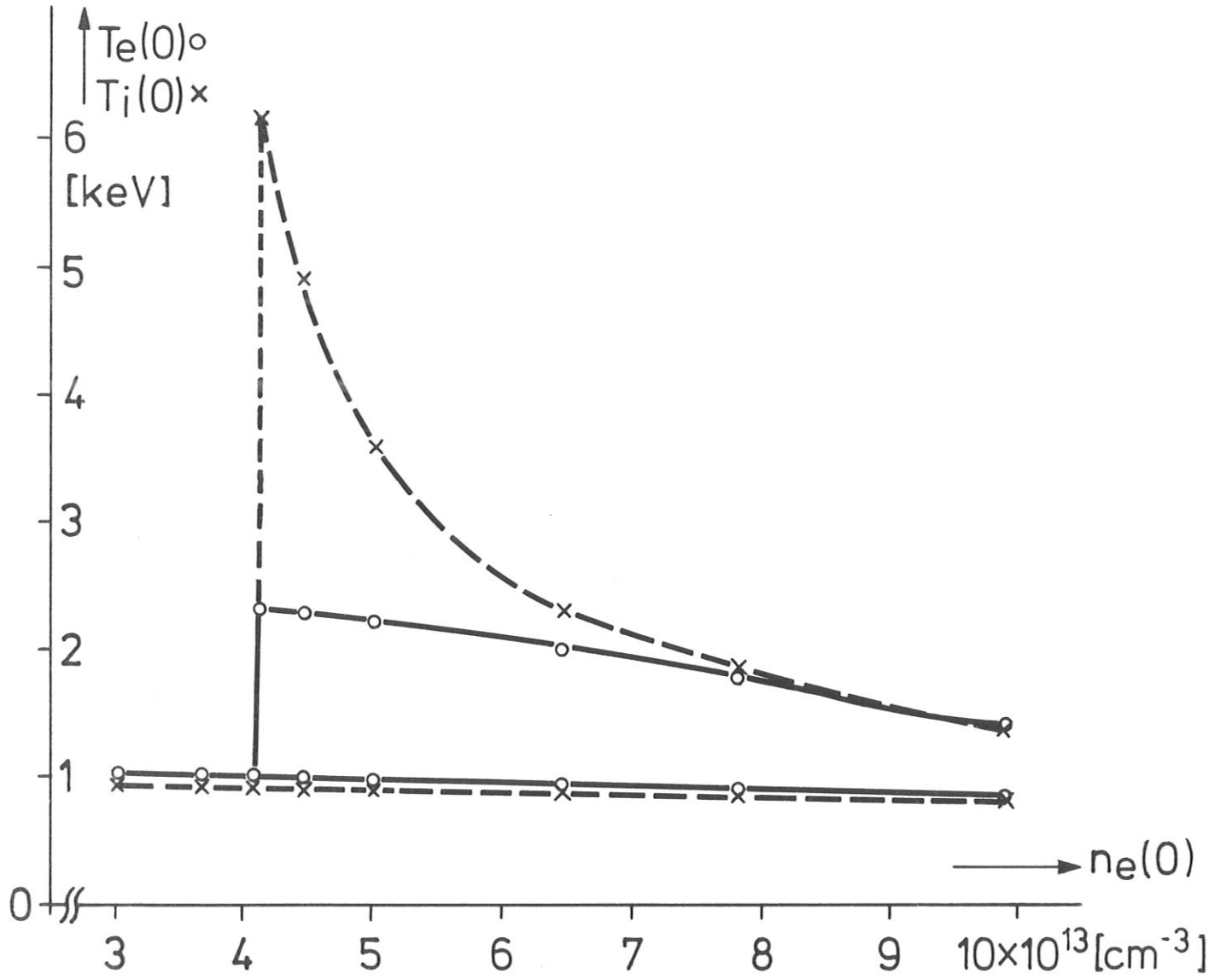

Fig.7

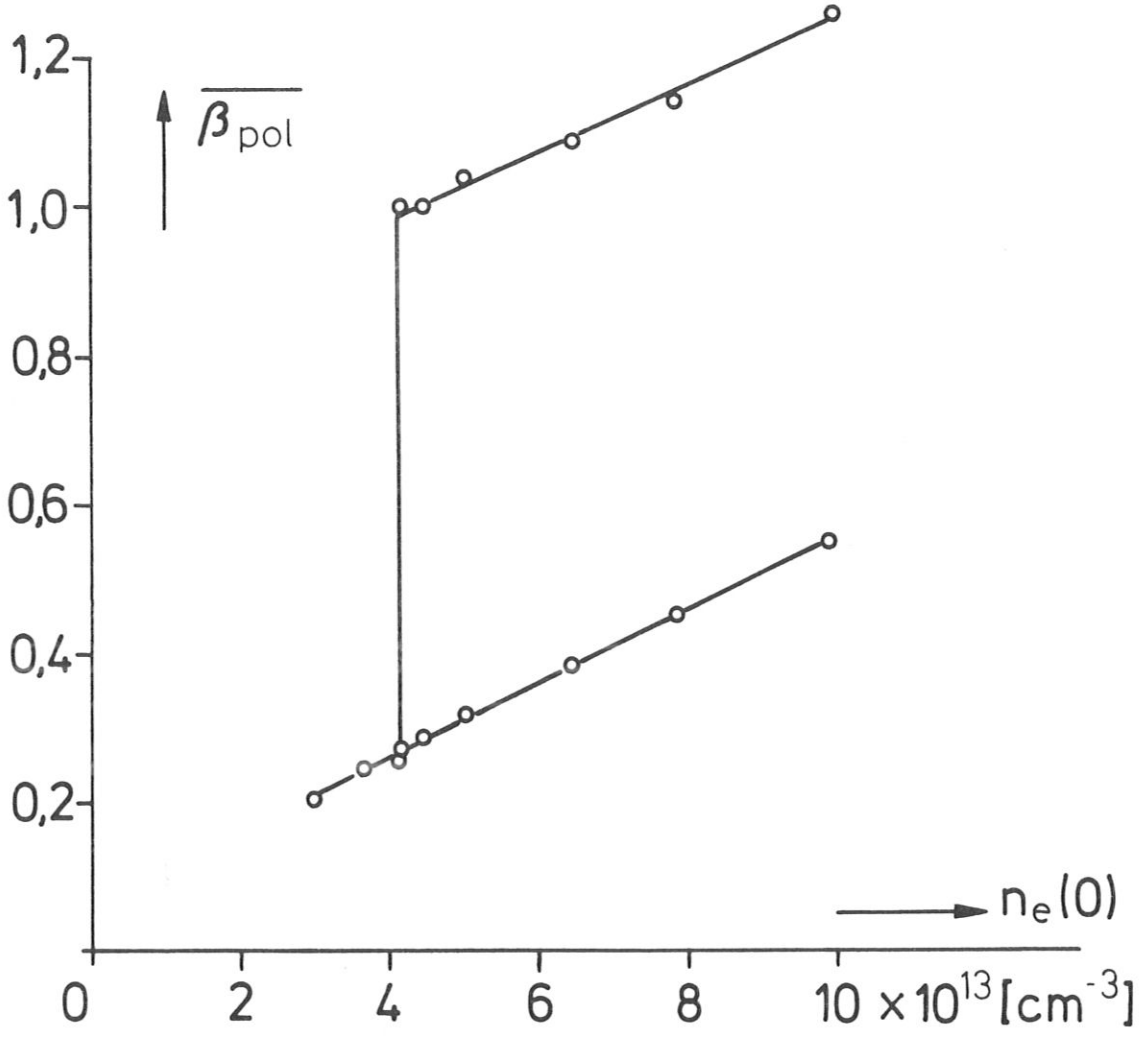
1,2
1,0
0,8
0,6
0,4
0,2
$\overline{\beta_{pol}}$
$n_e(0)$
0
2
4
6
8
10×10^{13} [cm^{-3}]

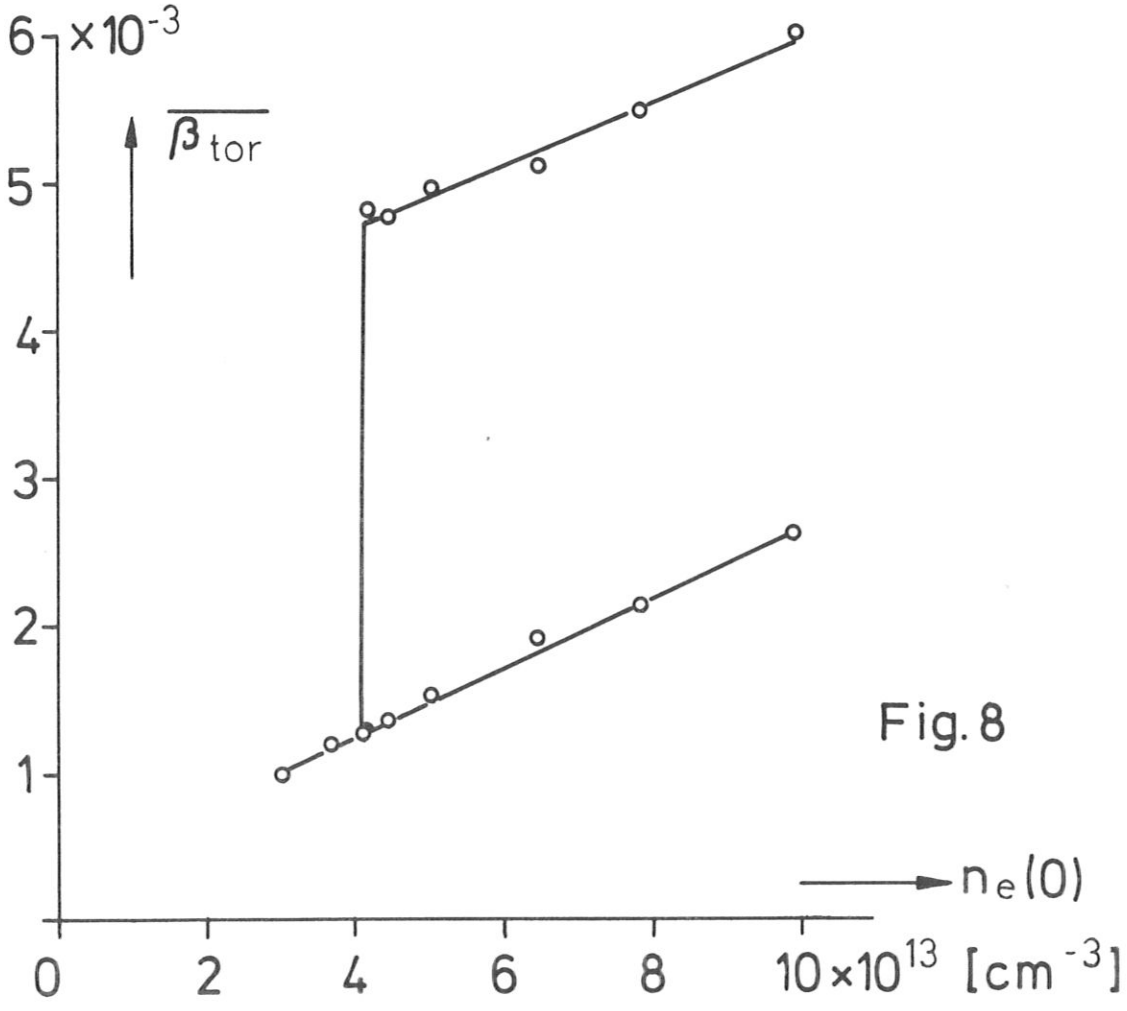
6
$\times 10^{-3}$
5
4
3
2
1
$\overline{\beta_{tor}}$
$n_e(0)$
0
2
4
6
8
10×10^{13} [cm^{-3}]

Fig. 8

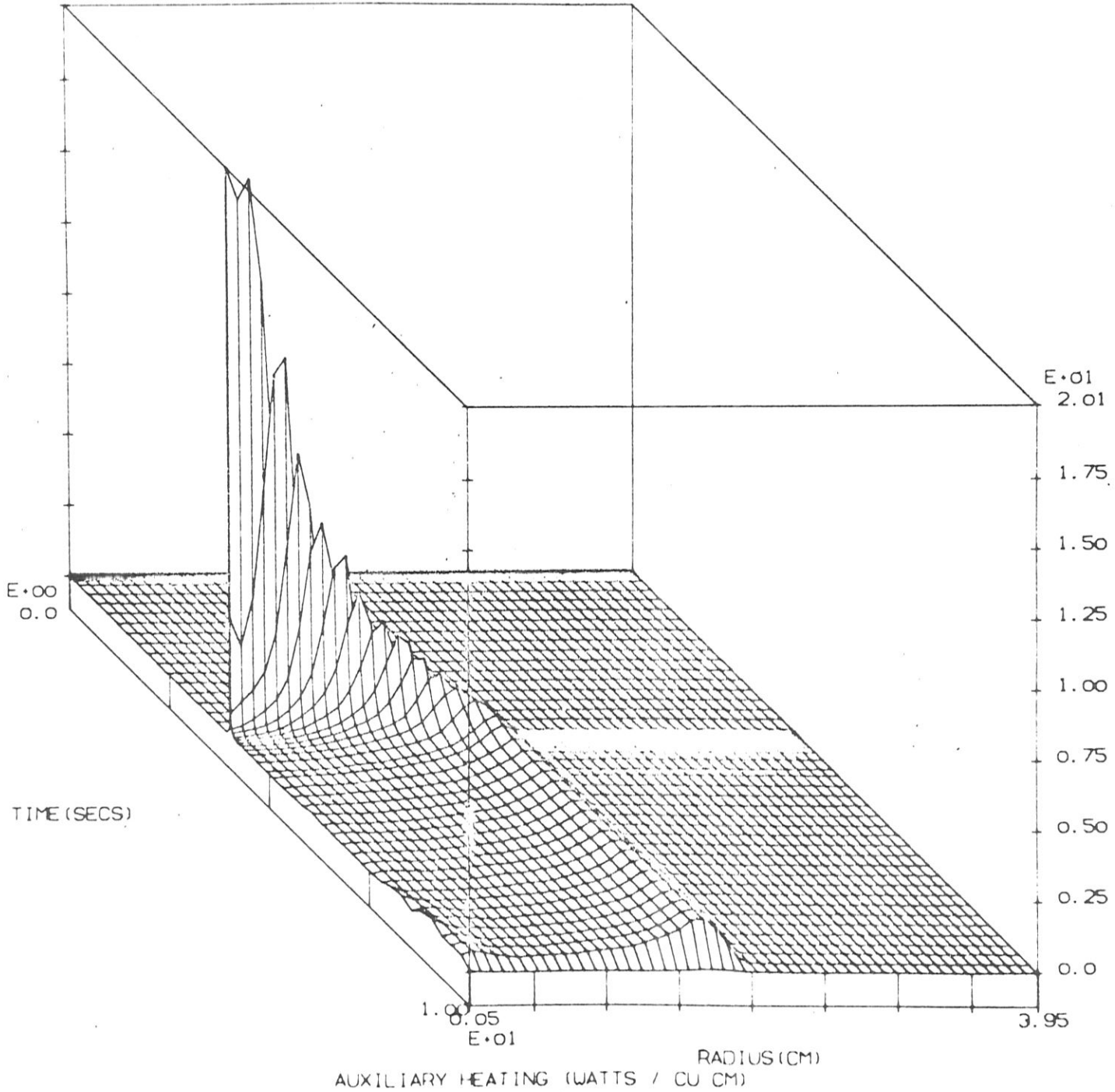
E·01
2.01
1.75
1.50
1.25
1.00
0.75
0.50
0.25
0.0
E·00
0.0
TIME(SECS)
1.00
0.05
E·01
3.95
RADIUS(CM)
AUXILIARY HEATING (WATTS / CU CM)

Fig.9

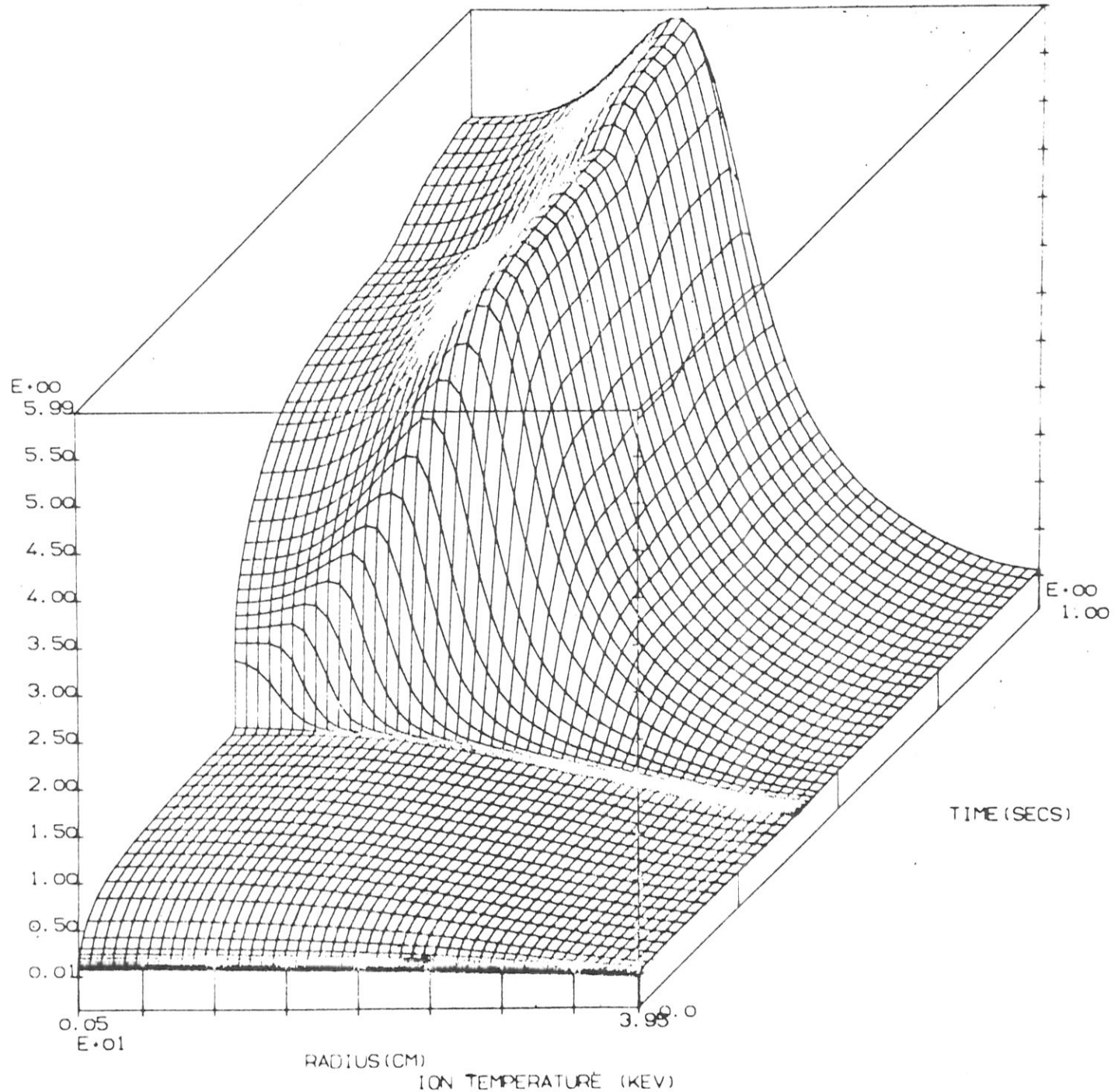
E·00
5.99
5.50
5.00
4.50
4.00
3.50
3.00
2.50
2.00
1.50
1.00
0.50
0.01
0.05
E·01
3.98
E·00
1.00
TIME (SECS)
RADIUS (CM)
ION TEMPERATURE (KEV)

Fig.10

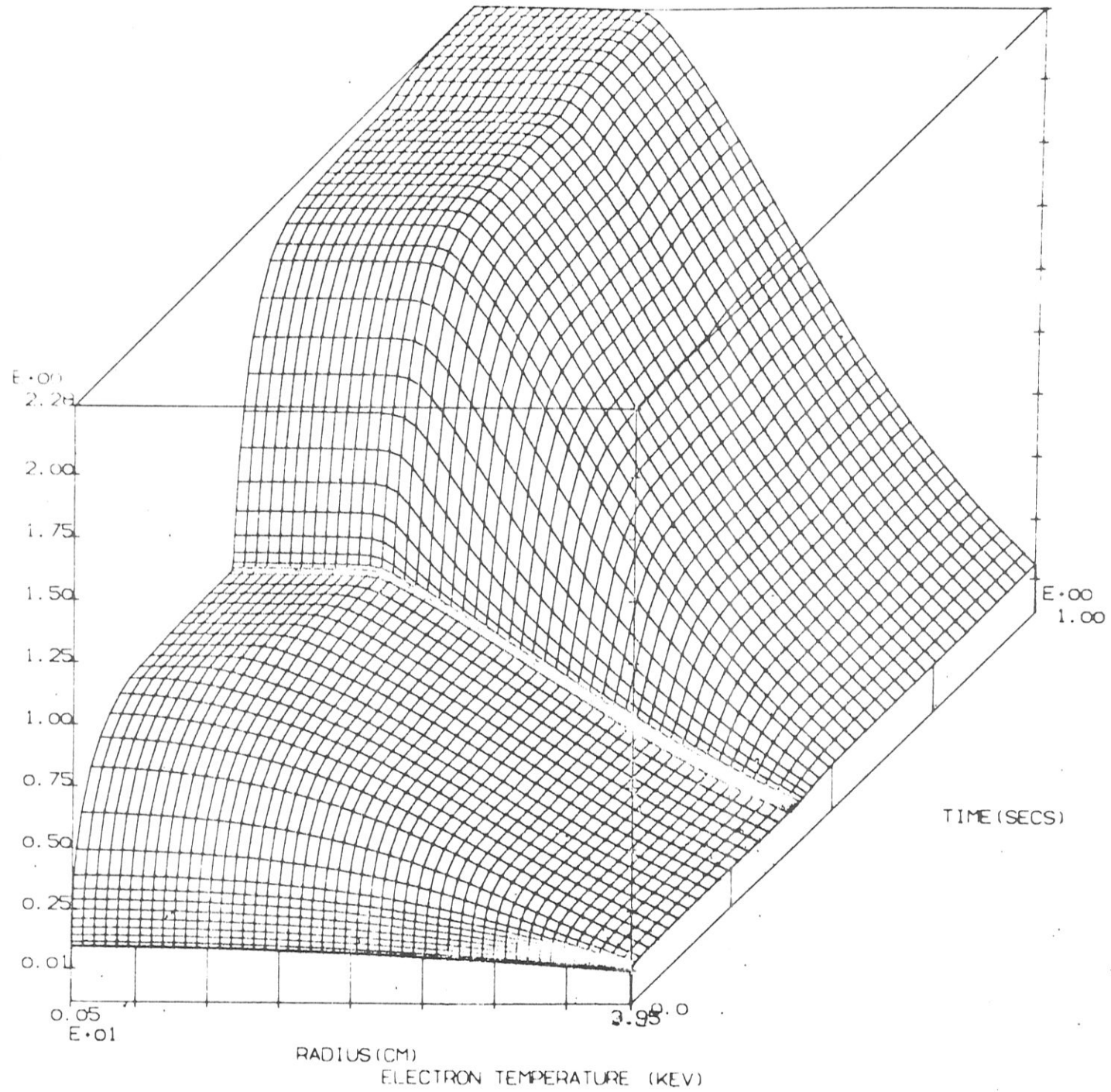
E·00
2.25
2.00
1.75
1.50
1.25
1.00
0.75
0.50
0.25
0.01
0.05
E·01
3.95
0.0
E·00
1.00
TIME(SECS)
RADIUS(CM)
ELECTRON TEMPERATURE (KEV)

Fig.11

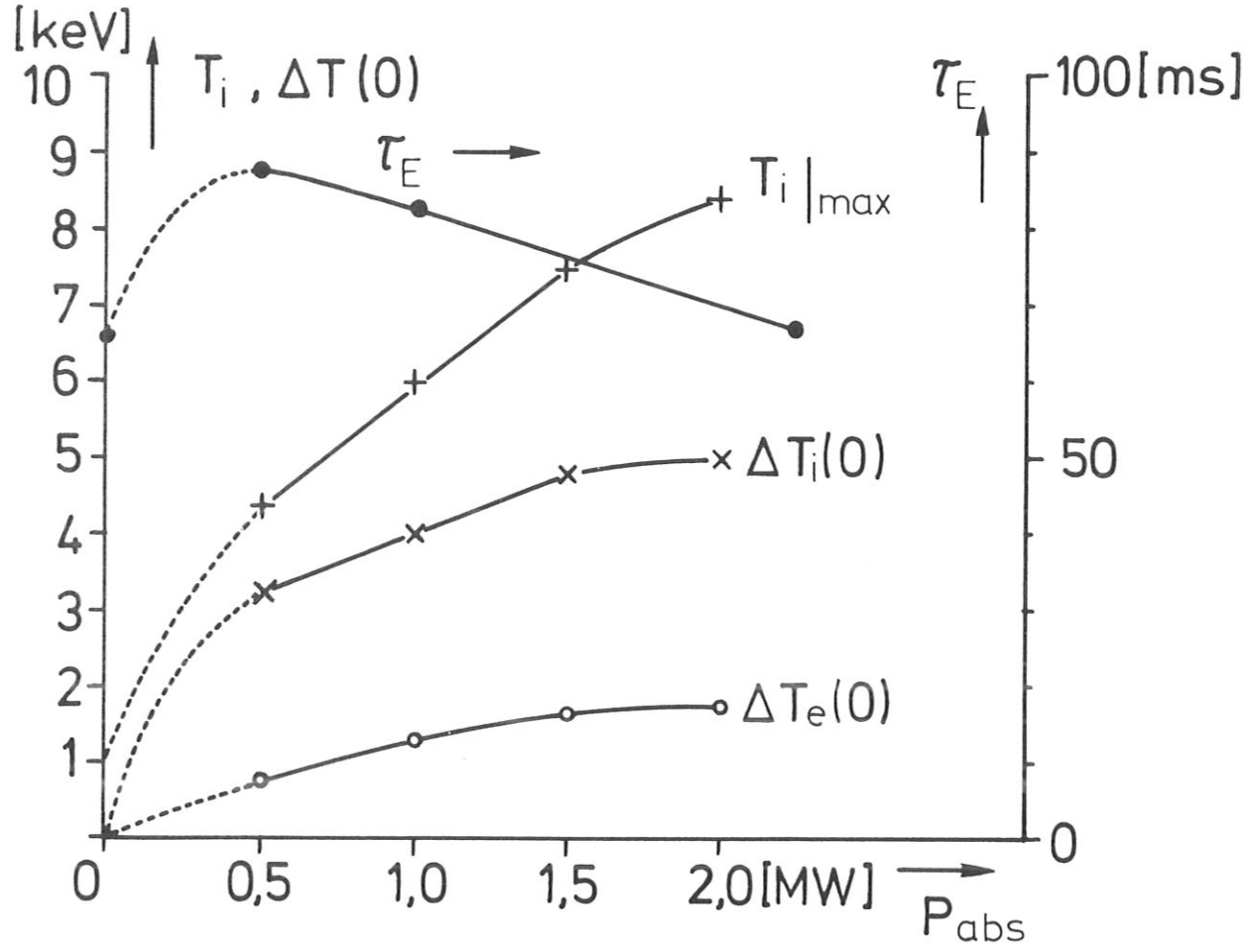
[keV]
T_i , $\Delta T(0)$
τ_E
τ_E
100[ms]
$T_i|_{max}$
$\Delta T_i(0)$
$\Delta T_e(0)$
50
0
0,5
1,0
1,5
2,0[MW]
P_{abs}

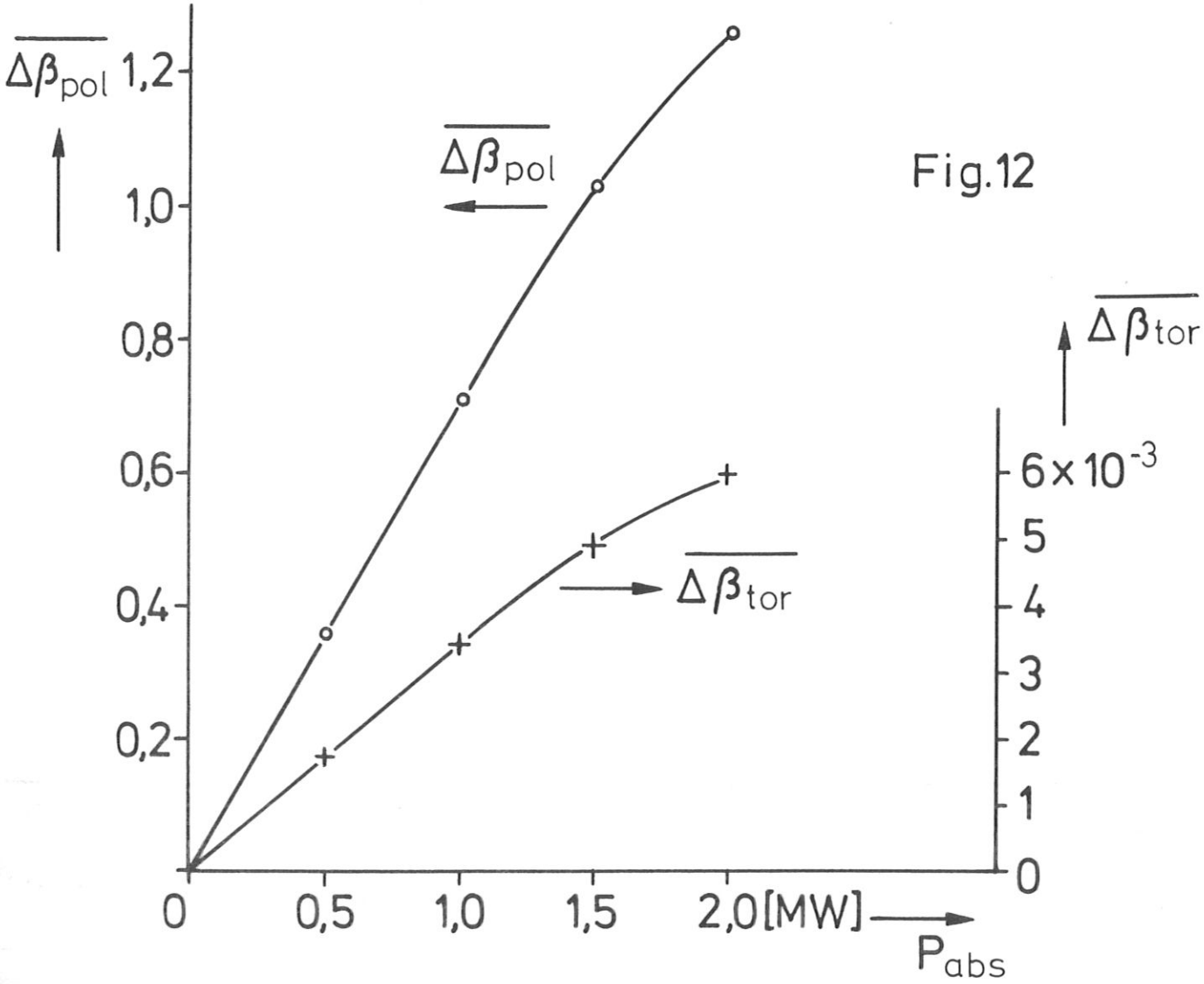
$\overline{\Delta\beta_{pol}}$
$\overline{\Delta\beta_{pol}}$
$\overline{\Delta\beta_{tor}}$
$\overline{\Delta\beta_{tor}}$
6×10^{-3}
0
0,5
1,0
1,5
2,0[MW]
P_{abs}

Fig.12

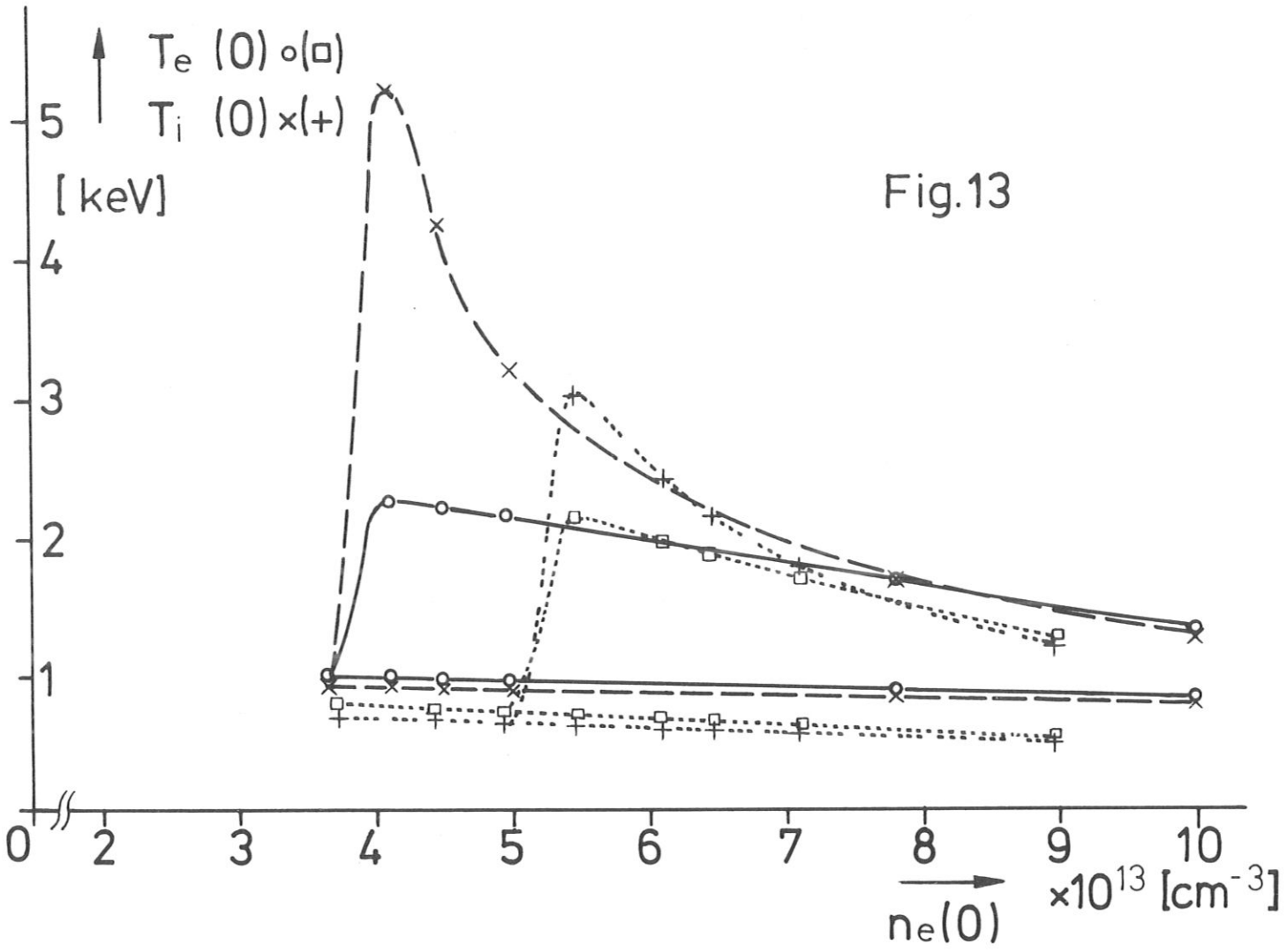
Te (0) ∘(□)
Ti (0) ×(+)
[keV]
5
4
3
2
1
0
2
3
4
5
6
7
8
9
10
ne(0)
×10^13 [cm^-3]

Fig.13

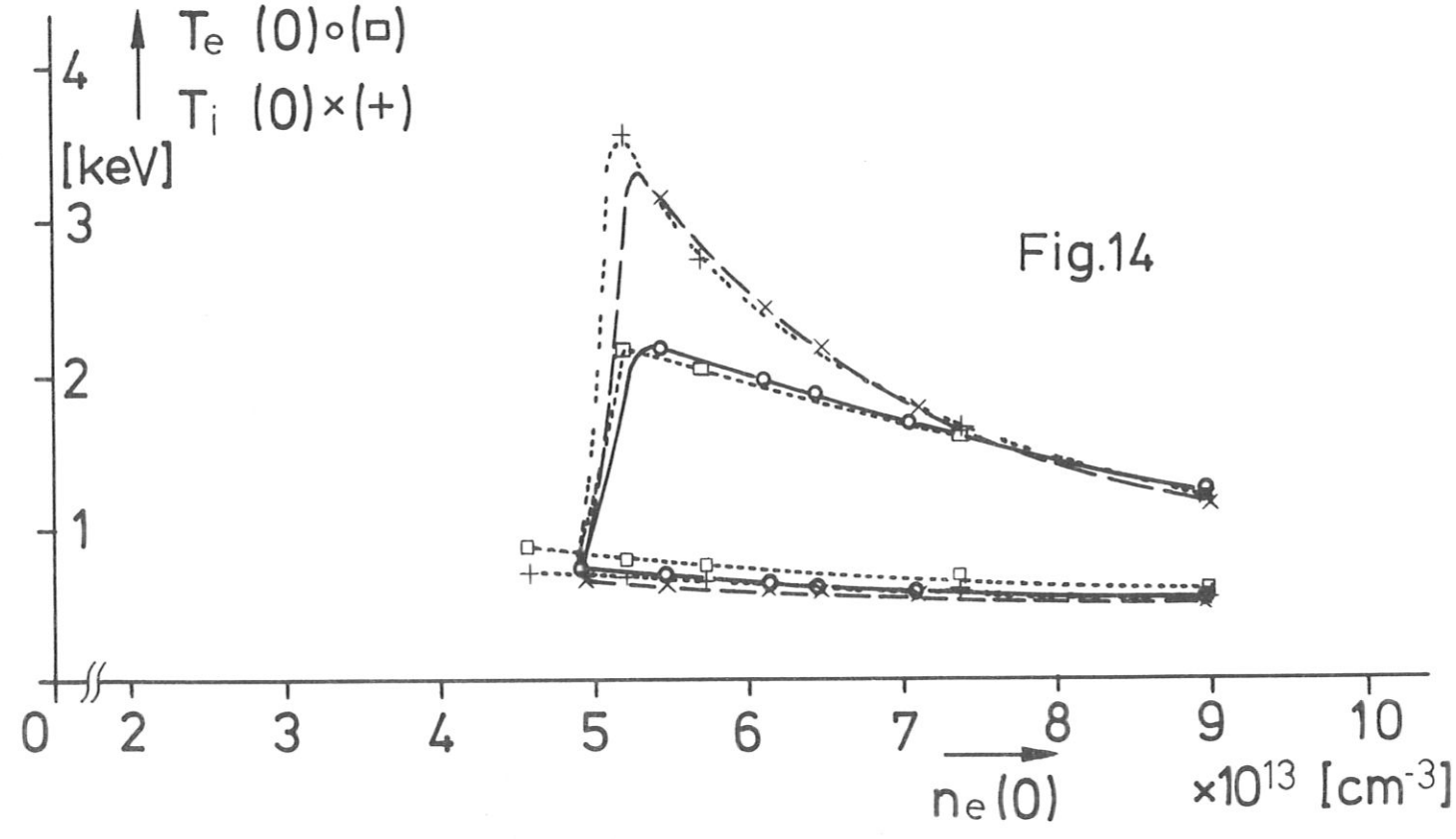
Te (0)∘(□)
Ti (0)×(+)
[keV]
4
3
2
1
0
2
3
4
5
6
7
8
9
10
ne(0)
×10^13 [cm^-3]

Fig.14

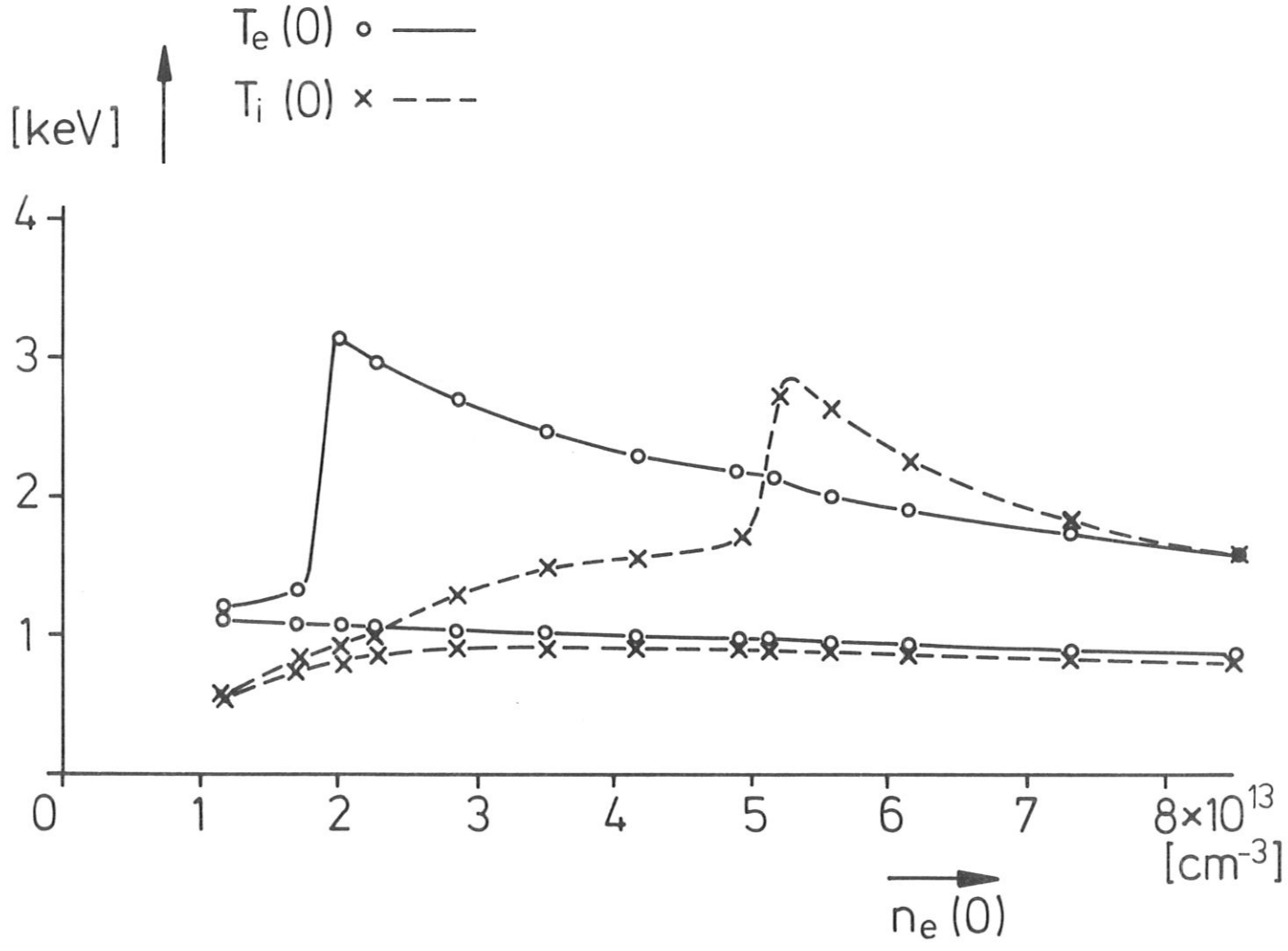

Fig. 15

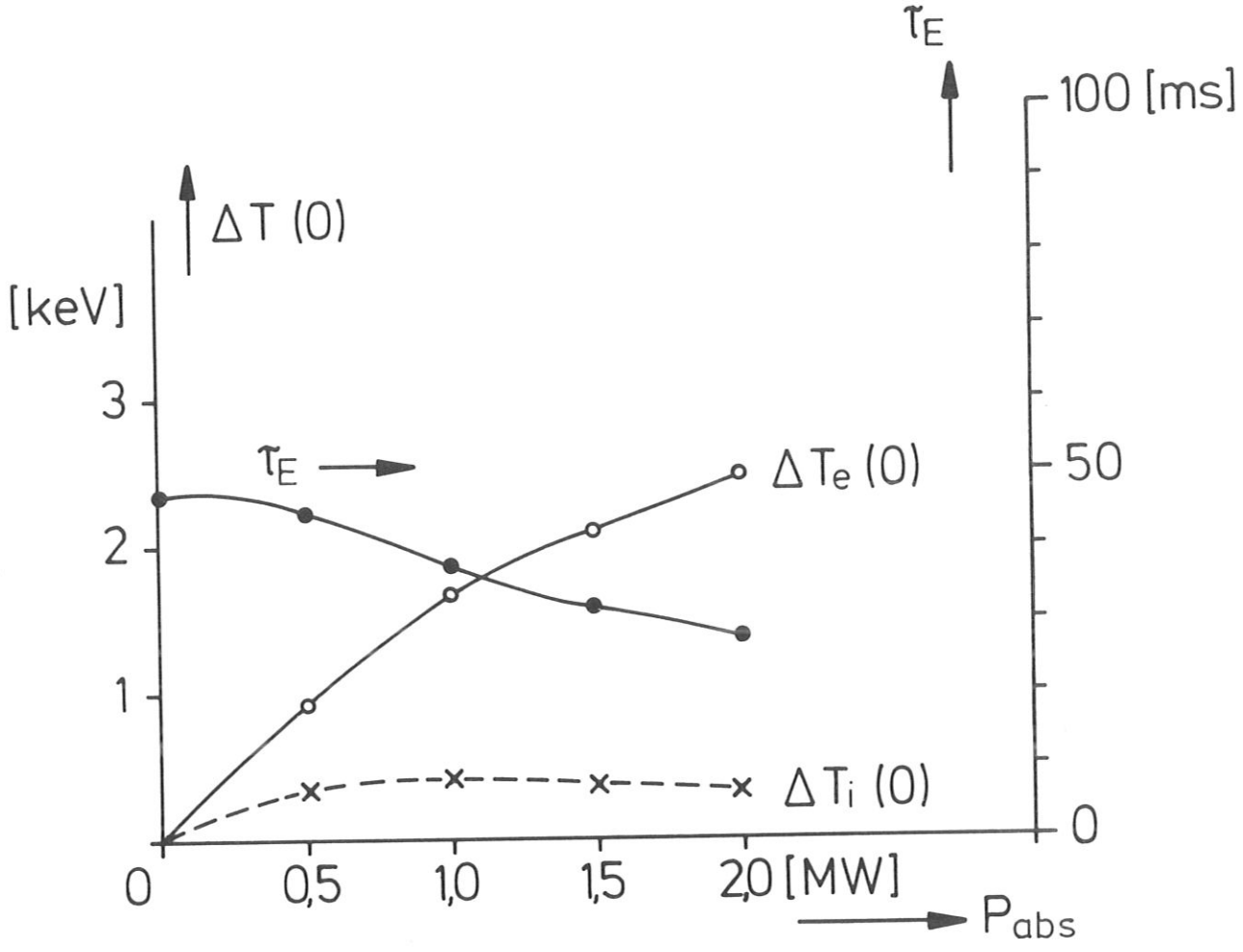
τ_E
100 [ms]
ΔT (0)
[keV]
3
2
1
τ_E
ΔT_e (0)
50
ΔT_i (0)
0
0
0,5
1,0
1,5
2,0 [MW]
P_{abs}

Fig. 16

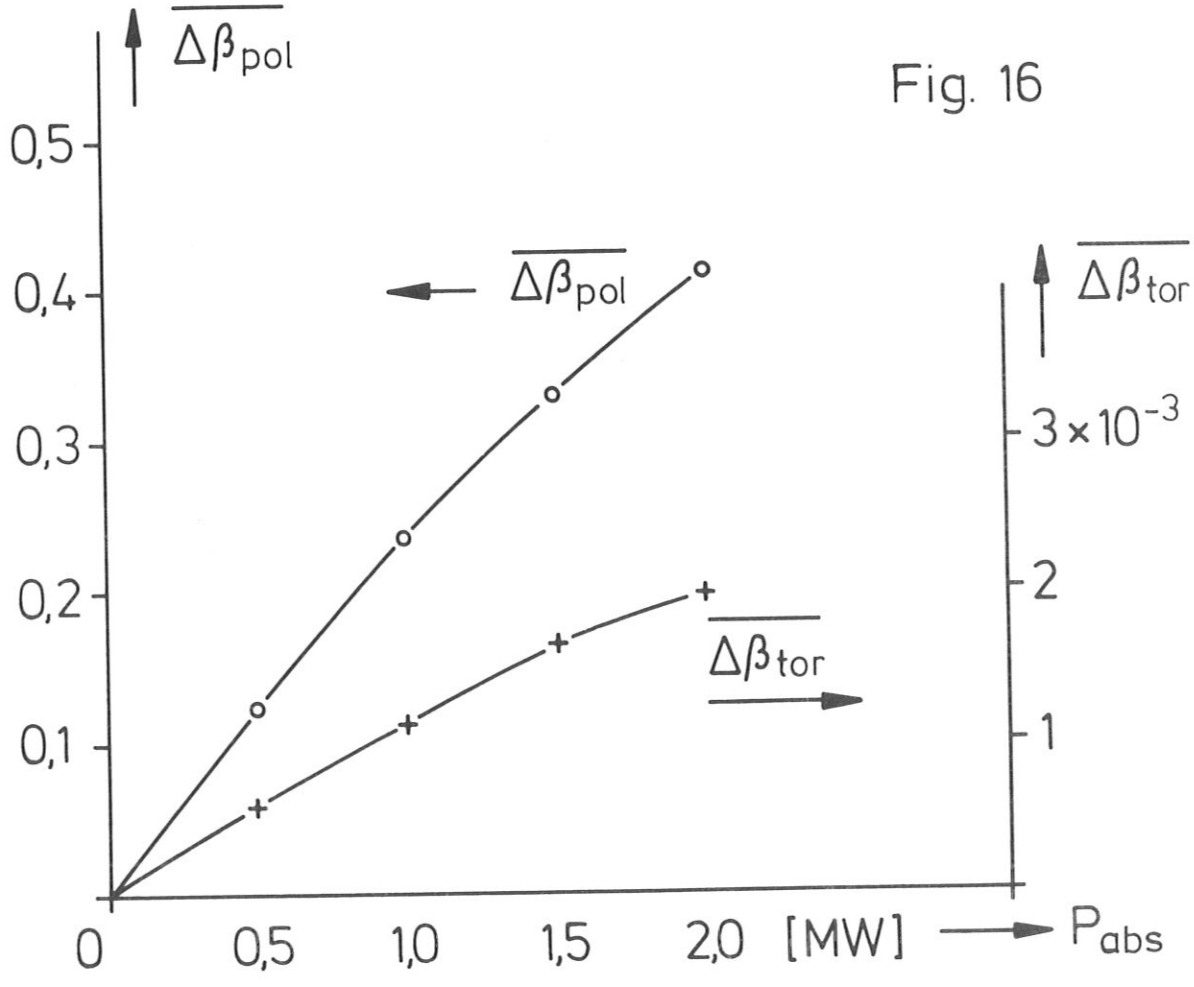
$\overline{\Delta\beta_{pol}}$
0,5
0,4
0,3
0,2
0,1
$\overline{\Delta\beta_{pol}}$
$\overline{\Delta\beta_{tor}}$
3×10^{-3}
2
$\overline{\Delta\beta_{tor}}$
1
0
0,5
1,0
1,5
2,0 [MW]
P_{abs}

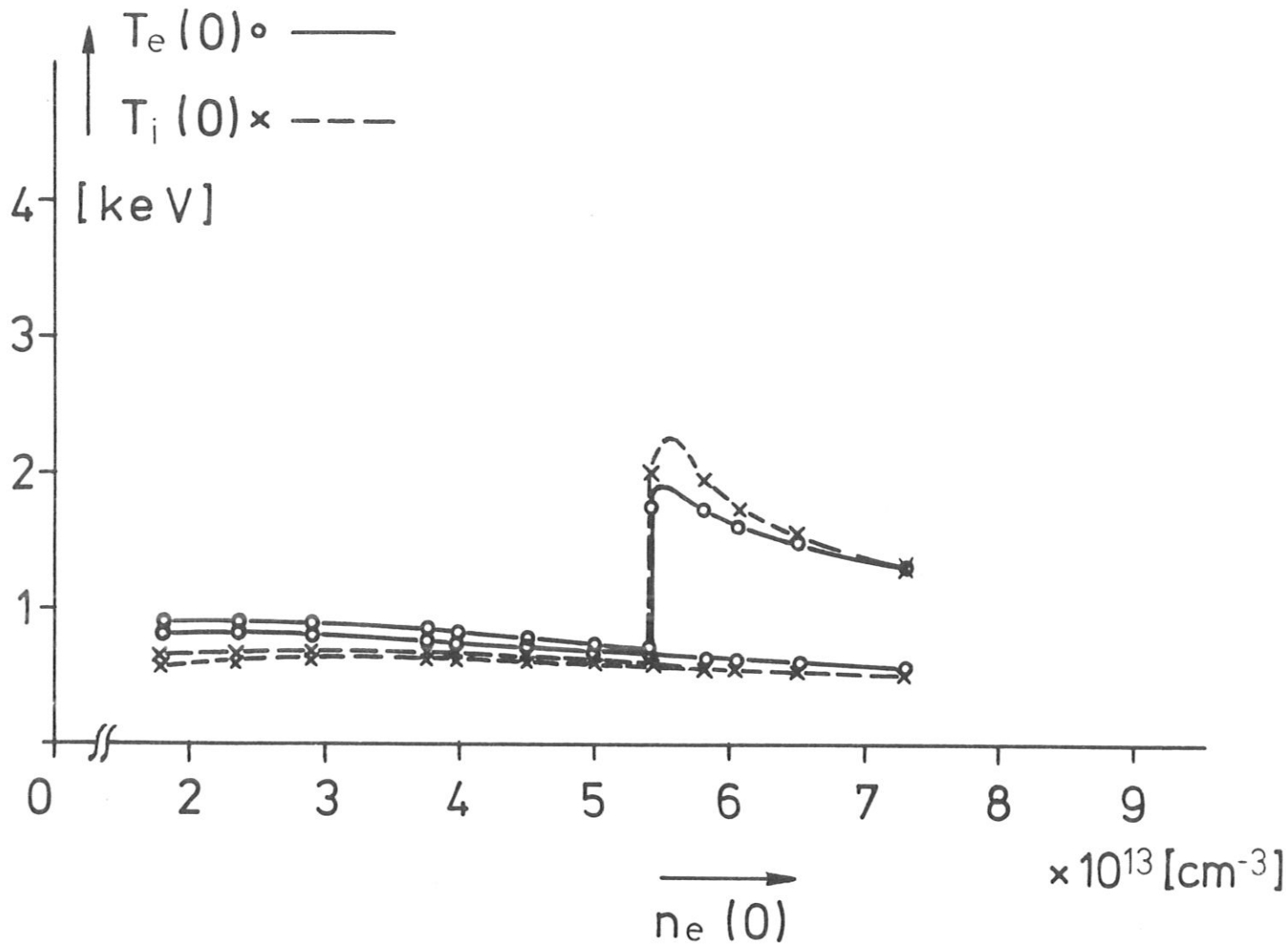
$T_e(0)$ ∘ ——
$T_i(0)$ × – – –
[keV]
4
3
2
1
0
2
3
4
5
6
7
8
9
$\times 10^{13}$ [cm^{-3}]
$n_e(0)$

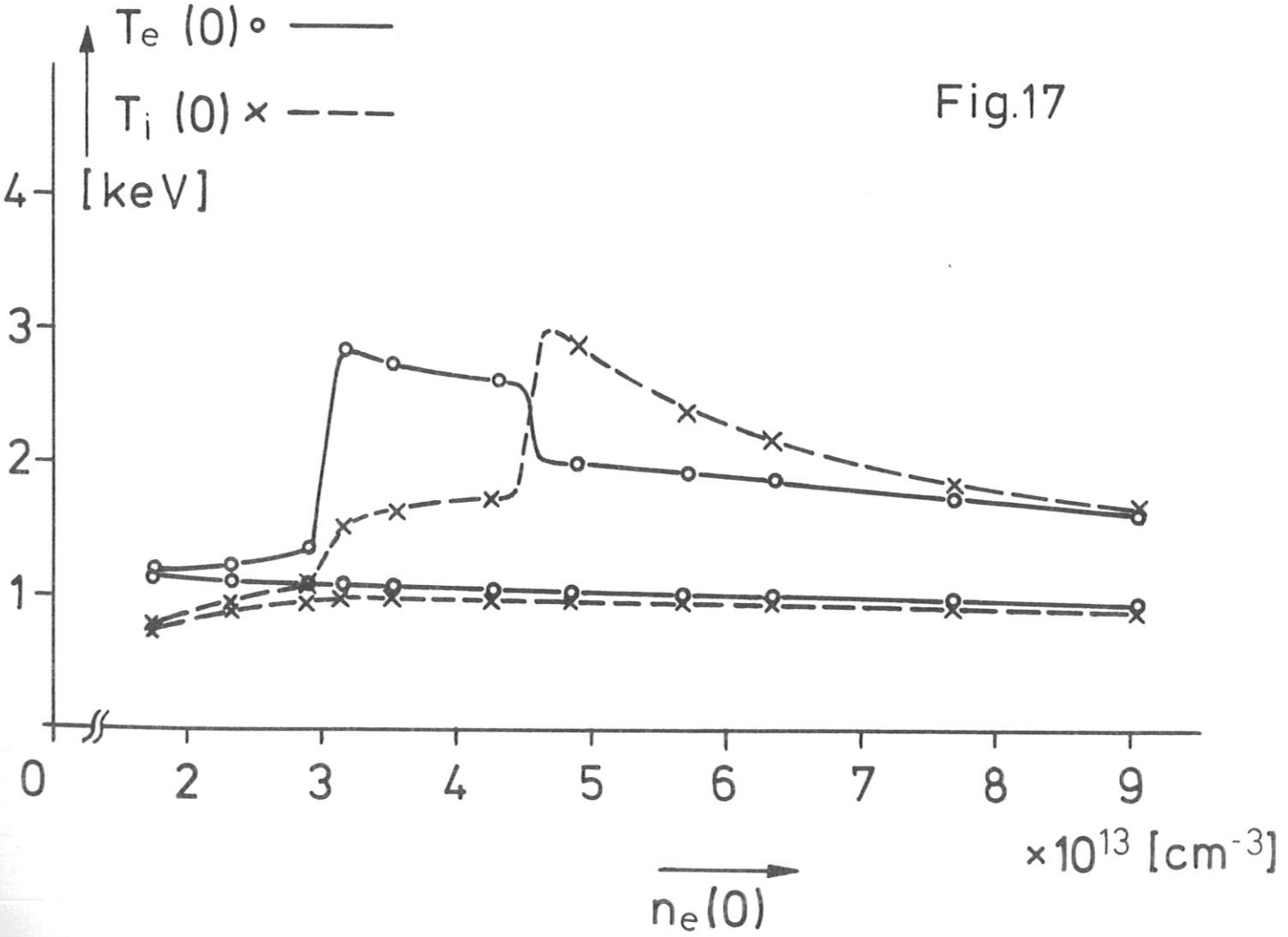
$T_e(0)$ ∘ ——
$T_i(0)$ × – – –
[keV]
4
3
2
1
0
2
3
4
5
6
7
8
9
$\times 10^{13}$ [cm^{-3}]
$n_e(0)$

Fig.17

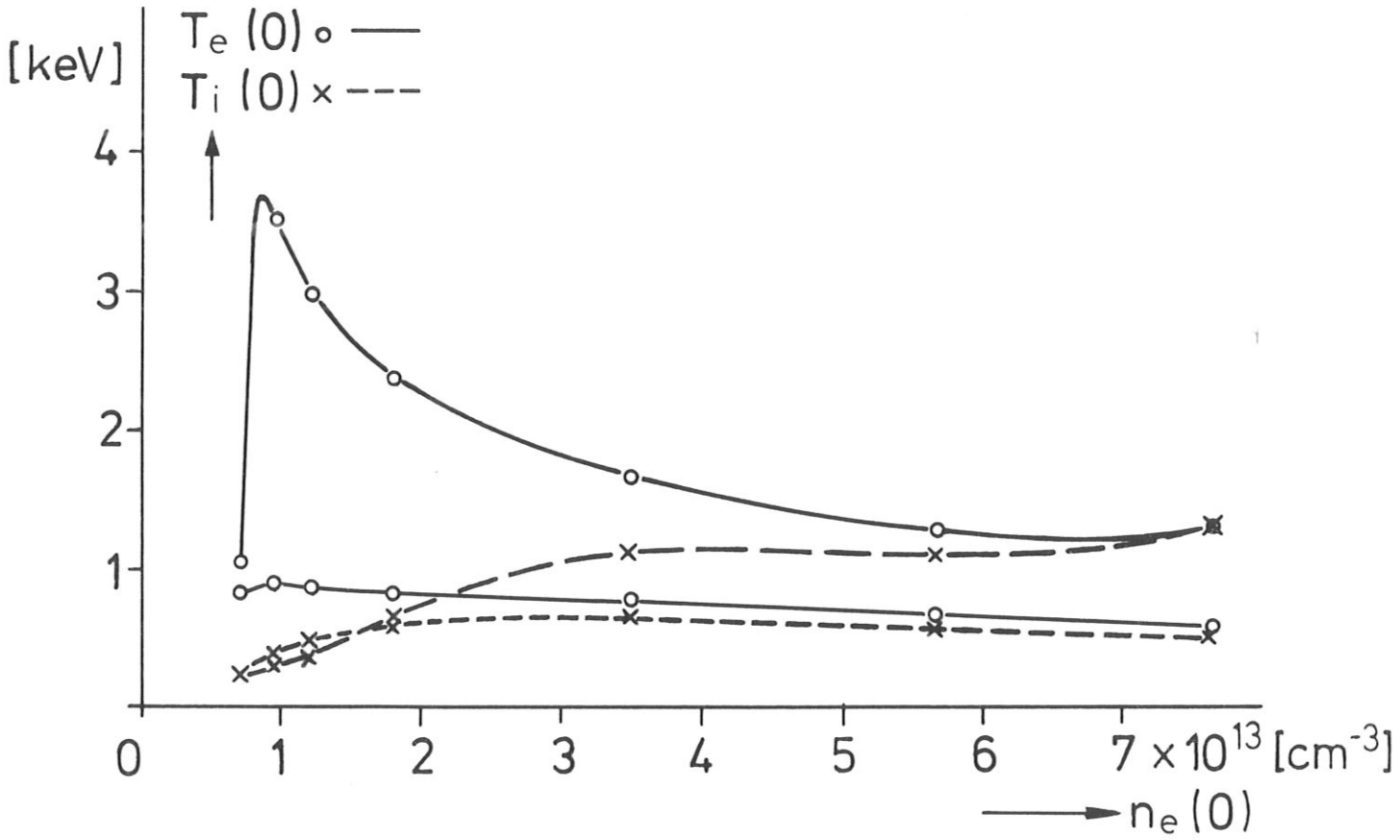

Fig. 18

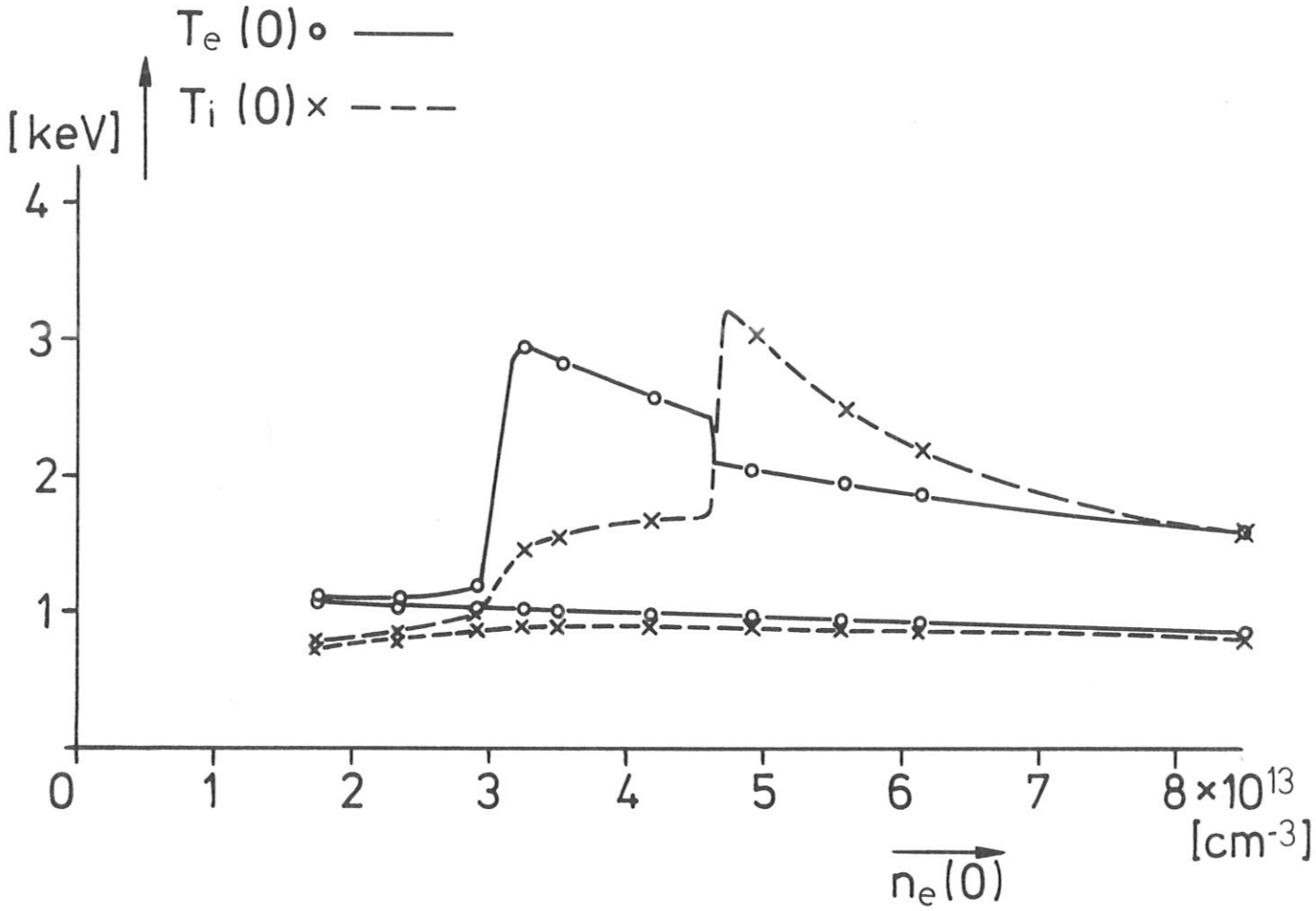
T_e (0) o ——
T_i (0) × – – –
[keV]
4
3
2
1
0
1
2
3
4
5
6
7
8×10^{13}
[cm^{-3}]
$\overrightarrow{n_e(0)}$

Fig.19

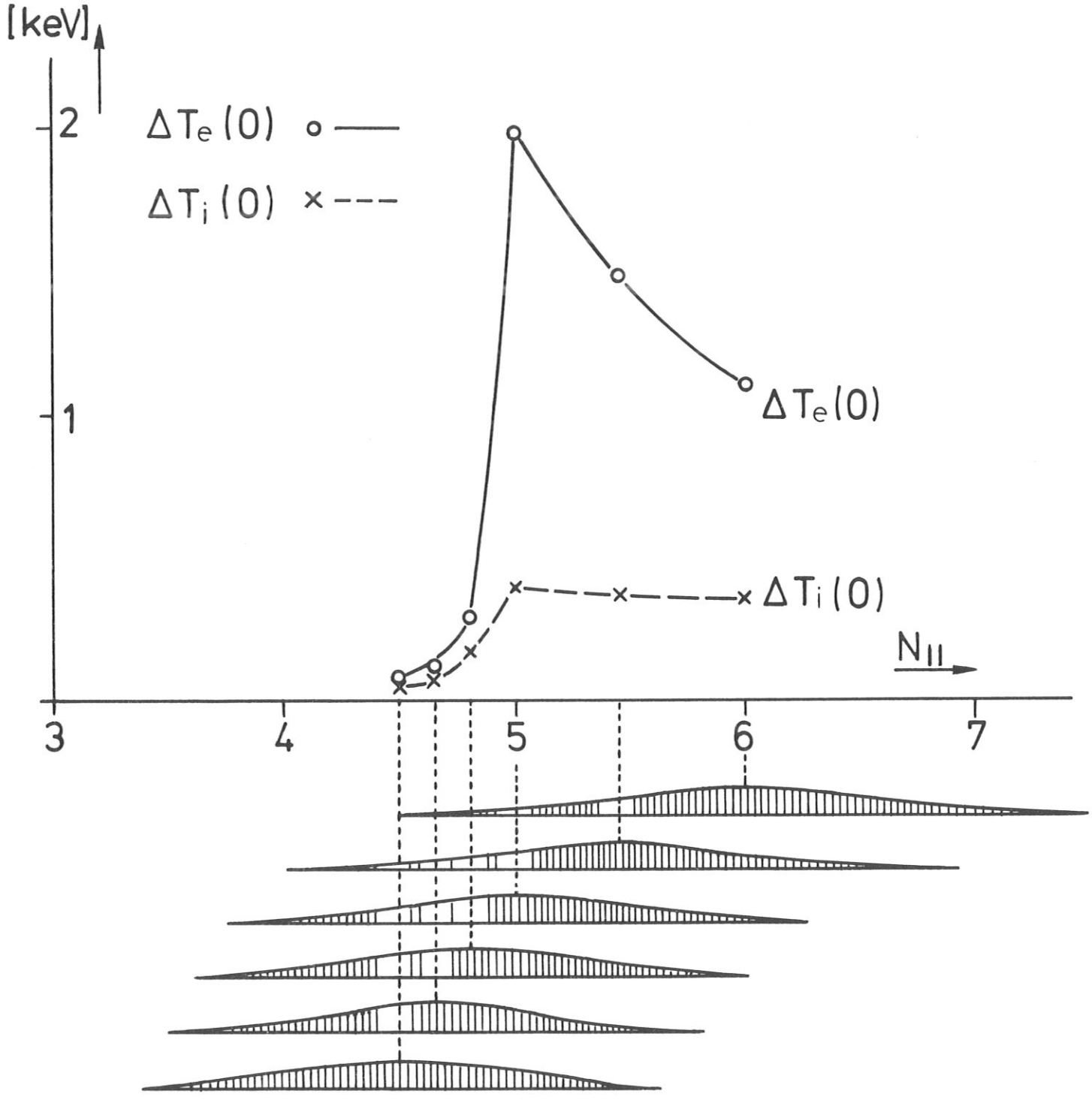

Fig.20